



## ORIGINAL ARTICLE

# Parvalbumin Interneurons Shape Neuronal Vulnerability in Blunt TBI

Akila Chandrasekar<sup>1</sup>, Florian olde Heuvel<sup>1</sup>, Lilla Tar<sup>1</sup>, Anna M. Hagenston<sup>2</sup>, Annette Palmer<sup>3</sup>, Birgit Linkus<sup>1</sup>, Albert C. Ludolph<sup>1</sup>, Markus Huber-Lang<sup>3</sup>, Tobias Boeckers<sup>4</sup>, Hilmar Bading<sup>2</sup> and Francesco Roselli <sup>1,3,5</sup>

<sup>1</sup>Department of Neurology, Ulm University, Ulm-DE 89081, Germany, <sup>2</sup>Department of Neurobiology—IZN, Heidelberg University, Heidelberg-DE 69120, Germany, <sup>3</sup>Department of Orthopedic trauma, Hand, Plastic and Reconstruction Surgery, Institute of Clinical and Experimental Trauma Immunology, Ulm University, Ulm-DE 89081, Germany, <sup>4</sup>Department of Anatomy and Cell Biology, Ulm University, Ulm-DE 89081, Germany and <sup>5</sup>Neurozentrum—Ulm University, Ulm-DE 89081, Germany

Address correspondence to Francesco Roselli, Department of Neurology, Ulm University, Center for Biomedical Research (ZBF), Helmholtzstrasse 8/2 (R1.44)-89081 Ulm-DE, Germany. Email: francesco.roselli@uni-ulm.de  [orcid.org/0000-0001-9935-6899](https://orcid.org/0000-0001-9935-6899)

## Abstract

Excessive excitation has been hypothesized to subsume a significant part of the acute damage occurring after traumatic brain injury (TBI). However, reduced neuronal excitability, loss of neuronal firing, and a disturbed excitation/inhibition balance have been detected. Parvalbumin (PV) interneurons are major regulators of perisomatic inhibition, principal neurons firing, and overall cortical excitability. However, their role in acute TBI pathogenic cascades is unclear. We exploited the chemogenetic Pharmacologically Selective Activation Module and Pharmacologically Selective Effector Module control of PV-Cre<sup>+</sup> neurons and the Designer Receptors Exclusively Activated by Designer Drug (DREADD) control of principal neurons in a blunt model of TBI to explore the role of inhibition in shaping neuronal vulnerability to TBI. We demonstrated that inactivation of PV interneurons at the instance or soon after trauma enhances survival of principal neurons and reduces gliosis at 7 dpi whereas, activation of PV interneurons decreased neuronal survival. The protective effect of PV inactivation was suppressed by expressing the nuclear calcium buffer PV-nuclear localisation sequence in principal neurons, implying an activity-dependent neuroprotective signal. In fact, protective effects were obtained by increasing the excitability of principal neurons directly using DREADDs. Thus, we show that sustaining neuronal excitation in the early phases of TBI may reduce neuronal vulnerability by increasing activity-dependent survival, while excess activation of perisomatic inhibition is detrimental to neuronal integrity.

**Key words:** chemogenetics, nuclear calcium, parvalbumin interneurons, traumatic brain injury

## Introduction

The acute phase of concussive and contusive traumatic brain injury (TBI) is characterized by pathogenic cascades linked to the physical damage of neurons and their uncontrolled excitation. Axonal stretching, membrane damage, and neuronal depolarization (triggered by the physical forces of the trauma) are known to cause glutamate release and/or failure in glutamate reuptake

system (Kaur and Sharma 2017). Elevated levels of glutamate in the extracellular space causes supraphysiological activation of glutamate receptors, which includes extrasynaptic N-methyl-D-aspartate (NMDA) receptors that are link to cell death pathways (Pohl et al. 1999; Hardingham et al. 2002; Hardingham and Bading 2010; Wroge et al. 2012; Hinzman et al. 2015; Samson et al. 2016). Toxic NMDA receptor signaling leads to calcium (Ca<sup>2+</sup>) overload,

followed by a loss of structural integrity, mitochondrial dysfunction, and metabolic disturbances, culminating in bioenergetics failure, and neuronal loss (Weber 2012; Hinzman et al. 2015; Sun et al. 2017; Bading 2017).

Despite the excitotoxic primary injury mechanisms, several lines of evidence suggest that reduced excitation may play a role in the pathophysiology of acute TBI: spreading depolarizations (pathophysiological features that closely follow TBI) have been reported to shift the excitation/inhibition balance towards increased inhibition (Sawant-Pokam et al. 2017). Neuronal responses to synaptic stimulation and sensory inputs are suppressed for several days after TBI (Johnstone et al. 2013, 2014; Allitt et al. 2016) and neuronal metabolism is decreased in the affected cortex (Dietrich et al. 1994). Interestingly, glutamatergic antagonists seem to be protective only in the very early phases of TBI and become detrimental to neuronal survival later (Pohl et al. 1999), suggesting that excitation-dependent neuroprotective signals may play a role in determining the vulnerability of neurons to TBI. Indeed, neuronal activity has been shown to increase resistance to oxidative stress and reduce vulnerability to apoptosis (Papadia et al. 2008; Zhang et al. 2007; 2009; Hardingham and Bading 2010; Léveillé et al. 2010). Thus, both excessive glutamatergic drive (excitotoxicity) and insufficient neuronal excitation may modulate the sensitivity of neurons to TBI-associated pathogenic cascades (as in other neurodegenerative conditions; Roselli and Caroni, 2015).

The net neuronal firing is determined not only by intrinsic properties, but is strongly influenced by the activity of glutamatergic synapses (together with the activation of nonsynaptic glutamatergic receptors), as well as by the inhibitory inputs (Isaacson and Scanziani 2011). GABAergic interneurons provide a homeostatic regulation of firing of excitatory neurons and shape the propagation of excitation in space and time (Wilent and Contreras 2005; Haider et al. 2013). Although selective loss of GABAergic subpopulations has been shown to take place in the chronic phase of TBI (Cantu et al. 2015), the functional role of inhibitory interneurons in acute TBI is yet to be fully elucidated.

Parvalbumin (PV)-positive interneurons constitute a subset of the cortical GABAergic population integrated in the local microcircuitry and providing perisomatic inhibition both in feedback and feed-forward architectures (Hu et al. 2014). PV interneurons regulate the overall output of the principal neurons (Defelipe et al. 1999; Cardin et al. 2009; Donato et al. 2013, 2015). In fact, strong activation of PV interneurons is sufficient to shut-down the firing of principal neurons (Atallah et al. 2012) and to curb pathological excitatory drive (Khoshkoo et al. 2017). Although PV interneurons appear to be affected by TBI (Vascak et al. 2017) and their derangement may contribute to the delayed-onset of post-traumatic hyperexcitability (Hsieh et al. 2017), their role in the acute phase after TBI remain unexplored. Is perisomatic inhibition a fundamental force in preventing excess excitation and excitotoxicity, or do PV interneurons instead exacerbate cortical silencing and neuronal vulnerability? Do PV interneurons represent an entry point to modulate the biological response of principal neurons to traumatic injury? To investigate these issues at a functional level, acute time-resolved manipulations of PV activity *in vivo* is necessary.

To these ends, we exploited a set of AAV-delivered tools, including engineered ion channels with orthogonal pharmacology (Pharmacologically Selective Activation Module [PSAM] and Pharmacologically Selective Effector Module [PSEM]; Magnus et al., 2011) and Designer Receptors Exclusively Activated by Designer Drug (DREADDs; Roth 2016) to control PV interneuron and principal neuron firing within discrete time windows in TBI. We have revealed that modulation of PV firing bidirectionally

modulates the acute response of principal neurons, their long-term viability and TBI-associated astrogliosis. Furthermore, we have demonstrated that neuroprotection of principal neurons through PV manipulation requires nuclear  $Ca^{2+}$  signals that are known to activate a neuroprotective gene program (Zhang et al. 2009). Taken together, our findings imply that early restoration of neuronal firing through microcircuit manipulation provides an innovative route to neuroprotection in TBI.

## Materials and Methods

### Mouse Lines

All experiments and procedures were approved by the local animal experimentation committee under the license no. 1222. B6;129P2-Pvalbtm1(cre)Arbr/J (henceforth PV-Cre) were a kind gift of Pico Caroni. PV-Cre mice were bred into homozygosity and maintained under standard husbandry conditions (24 °C, 40–60% humidity, 14/10 h light/dark cycle, unlimited access to water and food).

### Viral Vectors and Chemogenetic Agonists

AAV9 mediating the expression of PSAM (previously described; Magnus et al., 2011; Saxena et al., 2013) were obtained from Vector Biolabs (Malvern-PA, US) at the titers of  $9 \times 10^{12}$  viral genomes/mL using the following constructs: pAAV-pCAG-flox-PSAM(Leu41Phe, Tyr116Phe)5HT3-WPRE and pAAV-cbaflox-PSAM(Leu141Phe, Tyr116Phe) GlyR-WPRE, encoding the cation-permeable (activator PSAM, henceforth actPSAM), and the anion-permeable (inhibitory PSAM, henceforth inhPSAM) channels. AAV8 mediating the expression of the activating DREADD (pAAV-CaMKIIa-hM3D (Gq)-mCherry, corresponding to the plasmid #50476) were obtained from AddGene viral service. AAV2 mediating the expression of pAAV-flex-taCasp3-TEVp (previously reported; Yang et al. 2013) were obtained from the University of North Carolina (UNC) Vector Core facility. AAV2 mediating the expression of rAAV-GFP/Cre were obtained from UNC Vector Core facility. pAAV-hSyn-PV-nuclear localisation sequence (NLS)-mC, which drives the expression of PV-NLS-mCherry under control of the human synapsin promoter, was constructed by PCR-amplifying the PV-NLS-mCherry coding sequence from pAAV-CMV-PV-NLS-mCherry (Schlumm et al. 2013) and then subcloning it into a pAAV-hSyn expression plasmid. AAV1/2 particles were prepared as described previously (Zhang et al. 2007).

Since AAV2, AAV8, and AAV9 have been reported to have a similar neuronal infectivity in the cerebral cortex (Aschauer et al. 2013) and the viral suspensions were injected at high titer (in order to saturate the injection volume), the choice of the AAV pseudotype was due solely to the availability of high-quality, validated batches of viral vectors from different sources.

The PSAM agonist PSEM308 was obtained from Apex Scientific Inc. (Stony Brook-NY, USA) and was administered by intraperitoneal injection (i.p.) at the dose of 5 µg/g (dissolved in sterile saline) 30 min before TBI. The DREADD agonist Clozapine-N-Oxide (CNO) was purchased from Tocris (Wiesbaden-Nordenstadt, Germany) and administered i.p. at the dose of 5 µg/g (dissolved in sterile saline) 30 min before TBI.

### Intracerebral Injection of Viruses

Intracortical injection of AAVs was performed in mice at the age of P30–P35 as previously reported (Karunakaran et al., 2016). Mice undergoing surgery were administered buprenorphine (0.05 mg/kg; Reckitt Beckshire Healthcare, Beckshire, UK)

and meloxicam (1.0 mg/kg; Böhringer Ingelheim, Biberach an der Riß, Germany) 20 min before the procedure. After administration, mice were put under continuous isoflurane anesthesia (4% isoflurane in 96% O<sub>2</sub>) and positioned into a stereotactic frame. The scalp was incised at the midline and a burr hole was drilled (using a hand micro-drill) at the coordinates  $x = +2.0$ ,  $y = -2.0$ , corresponding to the somatosensory cortex. About 200–500 nL of the viral suspension (mixed with an equal volume of 1% Fast green solution) was injected using a pulled glass capillary, connected to a Picospritzer microfluidic device, over a span of 10 min. The capillary was kept in place for another 10 min to prevent backflow of the virus. The burr hole was left open to allow the bone to heal and the skin was sutured using a Prolene 7.0 surgical thread. After surgery, the animals were transferred to a recovery cage with a warmed surface and *ad libitum* access to food and water. Animals were administered additional doses of buprenorphine for the following 72 h and monitored for eventual neurological impairment.

### Experimental Traumatic Brain Injury Procedure and Experimental Groups

TBI was induced in mice by a modified closed, blunt weight-drop model (previously reported Flierl et al., 2009). Animals were pre-administered buprenorphine (0.1 mg/kg by subcutaneous injection) and put under sevoflurane anesthesia (5% sevoflurane in 95% O<sub>2</sub>). The scalp skin was incised on the midline to expose the skull and the animals were positioned in the weight-drop apparatus in which the head was secured to a holding frame. Using the 3-axis mobile platform in the apparatus, the impactor was positioned to the coordinates of the injection site ( $x = +2.0$ ;  $y = -2.0$ ,  $z = 0.0$ ). TBI was delivered by a weight of 120 g dropping from a height of 40 cm. A mechanical stop prevented a skull displacement (by the impactor) larger than 1.5 mm, in order to limit brain damage. Apnea time was monitored after TBI. Mice were administered 100% O<sub>2</sub> until normal breathing was restored. The scalp skin was sutured using the Prolene 6.0 surgical thread and the mice were transferred to a recovery cage (single-housed) with *ad libitum* access to food and water (Supplementary Fig. 1A). Additional doses of buprenorphine were administered every 12 h for the following 24 h after TBI. To reduce the suffering of the mice, their general state was checked using a score sheet (based on the NSS score, Flierl et al., 2009) to instate opportune measures or to euthanize the mice. Effort was made to minimize animal suffering and reduce the number of mice used.

For mice injected with the AAV9-PSAM/PSEM chemogenetics, six experimental groups were established: saline sham (mice with intracerebral injection of inhPSAM or actPSAM virus but injected with saline before undergoing sham surgery, henceforth sal-S), inhPSAM/PSEM sham (mice with intracerebral injection of the inhPSAM virus and injected with PSEM agonist before undergoing sham surgery, henceforth inh-S), actPSAM sham (mice with intracerebral injection of actPSAM virus but injected with PSEM agonist before undergoing sham surgery, henceforth act-S), saline TBI (mice with intracerebral injection of inhPSAM or actPSAM virus but injected with saline before undergoing TBI, henceforth sal-TBI), inhPSAM/PSEM-TBI (mice with intracerebral injection of inhPSAM virus and injected with PSEM agonist before undergoing TBI, henceforth inh-TBI) and actPSAM/PSEM-TBI (mice with intracerebral injection of actPSAM virus but injected with PSEM agonist before undergoing TBI, henceforth act-TBI). In order to establish if PV inactivation after TBI was effective, six experimental groups

were established (Supplementary Fig. 1B): saline sham (mice with intracerebral injection of inhPSAM virus but injected with saline before undergoing sham surgery, henceforth sal-S), inhPSAM/PSEM sham (mice with intracerebral injection of the inhPSAM virus and injected with PSEM agonist before undergoing sham surgery, henceforth inh-S), saline TBI (mice with intracerebral injection of inhPSAM virus but injected with saline before undergoing TBI, henceforth sal-TBI), inhPSAM/PSEM-TBI acute (pre) agonist administration (mice with intracerebral injection of inhPSAM virus and injected with PSEM agonist before undergoing TBI, henceforth inh-TBI), inhPSAM/PSEM-TBI acute (post) agonist administration (mice with intracerebral injection of inhPSAM virus and injected with PSEM agonist 30 min after TBI and 8 h after TBI, such that the inhibition of PV interneurons was maintained for a total of 24 h, henceforth, inh-24 h-TBI) and inhPSAM/PSEM-TBI subacute agonist administration (mice with intracerebral injection of inhPSAM virus and injected with PSEM agonist starting 2 dpi up to 4 dpi (2 doses daily), such that the inhibition of PV interneurons was maintained for a total of 72 h, henceforth, inh-72 h-TBI). The experiment in which the PV interneurons were ablated had 4 groups: GFP sham (intracerebral injection of AAV2-GFP and sham surgery, henceforth GFP-S), ablation sham (intracerebral injection of AAV2-Caspase-3 and sham surgery, henceforth abl-S), GFP-TBI (intracerebral injection of AAV2-GFP and TBI, henceforth GFP-TBI), and ablation TBI (intracerebral injection of AAV2-Caspase-3 and TBI, henceforth abl-TBI). The chemogenetic stimulation (AAV8-DREADD(Gq), CaMKIIa promoter) of ipsi or contralateral principal neurons was explored with an experimental design including 7 groups: mice expressing the DREADD(Gq) expressed on the ipsilateral side but saline injection before sham surgery (henceforth Gq-sal-S), mice expressing the DREADD(Gq), injected with CNO but subject to sham surgery (henceforth Gq-CNO-S), mice expressing the DREADD(Gq) expressed on the ipsilateral side but saline injection before TBI (henceforth Gq-sal-TBI), mice expressing DREADD(Gq) virus on the ipsilateral side and administered the CNO agonist before TBI (henceforth Gq-CNO-TBI), mice expressing DREADD(Gq) virus on the ipsilateral side, administered CNO, subject to sham surgery but for which the contralateral cortex was assessed (henceforth Gq-contralateral-CNO-S), mice injected with DREADD(Gq) virus on the ipsilateral side, injected with saline before TBI delivered on the contralateral side (henceforth Gq-contralateral-TBI), mice expressing DREADD Gq virus on the ipsilateral side and administered CNO before TBI on the contralateral side (henceforth Gq-contralateral-CNO-TBI).

Mice injected with the AAV1/2-PV-NLS-mCherry virus along with the inhPSAM inhibitor virus were divided in 3 groups: injected with PV-NLS-mCherry and inhPSAM viruses, subject to sham surgery; injected with PV-NLS-mCherry and inhPSAM viruses but administered saline before TBI and injected with PV-NLS-mCherry and inhPSAM viruses and administered PSEM agonist before TBI (Supplementary Fig. 2).

### Immunostaining

For immunostaining, mice were intracardially perfused. Animals were terminally anesthetized with ketamine/xylazine and fixed (25 mL ice-cold PBS followed by 50 mL 4% PFA in PBS, pH 7.4) at 3 h or 7 dpi. The brain was carefully extracted and post fixed in 4% PFA for 18 h and thereafter washed in PBS and cryoprotected in 30% sucrose in PBS. Cryoprotected brains were embedded in OCT (TissueTek, Sakura). 40 µm thick free-floating sections, spanning the injection/TBI site (identified by fast green) were cut in a

cryostat, collected in PBS and immunostaining was done based on the following protocol: sections were blocked in a blocking buffer (3% BSA, 0.3% Triton in PBS) for 2 h at 24 °C on a rotary shaker. Following blocking an appropriate mix of primary antibodies (chicken anti-GFP, 1:000, Abcam; goat anti-PV, 1:1000, Swant; rabbit anti-phosphorylated S6 (Ser235/236) 1:200, Cell Signaling Technology; mouse anti-NeuN, 1:100, Millipore; rabbit anti-c-Fos, 1:500, Santa Cruz Biotechnologies; mouse anti-RFP, 1:500, cell Biolabs; rabbit anti-cleaved caspase-3, 1:400, Cell Signaling Technology; mouse anti-GFAP, 1:400, Sigma; rabbit anti-GFAP, 1:500, Abcam or fluorescently-conjugated Bungarotoxin, BTX-555, 1:500, Thermo Fisher) were diluted in blocking buffer and incubated for 48 h at 4 °C. Sections were then washed in PBS for 3 × 30 min and incubated in the appropriate mix of secondary antibodies (Alexa-conjugated donkey anti-mouse, donkey anti-goat, donkey anti-rabbit, donkey anti-chicken, 1:500, Invitrogen), together with, whenever appropriate, the DNA dye TOPRO-3 (1:1000, Invitrogen), diluted in blocking buffer for 2 h at 24 °C. After further washing the sections for 3 × 30 min in PBS, the sections were mounted on coverslips and onto the slides using FluoroGold Plus (Invitrogen).

### Confocal Imaging and Image Analysis

Confocal images were acquired using an LSM-700 (Carl Zeiss AG) inverted microscope, fitted with a 20× air or 40× oil objective. Tile-scans of 5×3 were acquired to cover the full span of the injury site and the full cortical thickness. The images were acquired in a 12-bit format. Imaging parameters (laser power, photomultiplier voltage, digital gain, and offset) were established with the goal of preventing saturation in target structures while obtaining a lowest signal intensity of at least 150 (in arbitrary units). Imaging parameters were kept constant across different specimens.

For pS6 fluorescence intensity analysis, confocal stacks composed of 10 optical sections (acquired at the same depth in the tissue section) were collapsed in maximum-intensity projections using the ImageJ software. Neurons were identified based on their morphology, size and positive immunostaining for the neuronal marker (NeuN). A target region of 40 000 μm<sup>2</sup> was considered for each section, spanning the cortical layer II–III and centered on the axis of the injury site. Regions of Interest (ROIs) encompassing the cellular soma (excluding the nucleus) were manually drawn for each neuron in the target region and the integrated average fluorescence intensity was logged. A minimum of 300 neurons (layer II–III) from 3 distinct tissue sections from each of 3–5 mice were quantified. The intensity of pS6 in PV interneurons was also measured separately. The median fluorescence intensity of pS6 was computed.

For the counting of c-Fos<sup>+</sup> neurons, confocal stacks of 10–12 optical sections were collapsed in maximum-intensity projections in ImageJ and a threshold was set for the resulting images, to establish a reproducible criterion to distinguish c-Fos<sup>+</sup> neurons from c-Fos<sup>-</sup> neurons. A ROI (2.5 × 10<sup>6</sup> μm<sup>2</sup>) was then traced in layer II–III and the number of c-Fos<sup>+</sup> cells were counted. The number of c-Fos<sup>+</sup> PV interneurons were also separately counted.

For the measurement of NeuN<sup>+</sup> cells, 5 × 3 composite tile-scans of confocal stacks were acquired with the 20 × objective to image the injury site and the surrounding penumbral and perilesional areas. Confocal stacks of 5–6 optical sections (at the same depth) were collapsed in maximum-intensity projections in ImageJ. Multiple ROIs were considered: the “lesion core” (76 000 μm<sup>2</sup>) ROI was positioned centered on the axis of

the injury site and 2 “penumbral” (48 000 μm<sup>2</sup>) ROIs were located at 400 μm from the lesion axis, bilaterally, in correspondence of the layer II–III (Supplementary Fig. 3A). A third ROI was considered for the experiment with the NLS-PV-mCherry AAV2; this ROI (76 000 μm<sup>2</sup>) was located 700 μm away from the lesion axis (Supplementary Fig. 3B). In these ROIs, the number of NeuN<sup>+</sup> cells (or of mCherry<sup>+</sup> or GFP<sup>+</sup> cells) were manually counted. At least 3–5 tissue sections were analyzed from each of 3–6 mice per experimental group.

### Statistics

Statistical analysis was performed with the GraphPad Prism software suite. Neuronal counts and fluorescence intensities were compared by one-way analysis of variance with Tukey correction for multiple comparisons. The whiskers in the box and whiskers plot were set between 10% and 90%. For the fluorescence intensity of pS6 in PV interneurons and the number of c-FOS<sup>+</sup> cells in PV interneurons, nonparametric t-test with Mann–Whitney correction was performed to compare the 2 groups (sham vs. TBI). Nonparametric t-test with Mann–Whitney correction was also used to compare the number of PV interneurons in mice injected with AAV2-GFP versus AAV2-Caspase 3. The values for the neuronal counts are reported as mean ± SD. For the fluorescence intensities the median values and the interquartile range are reported. Statistical significance was set at  $P < 0.05$ .

## Results

### PV Interneurons Modulate the Acute Response of Principal Neurons to TBI

First, we explored the recruitment of PV interneurons in the early stages after blunt TBI. To this end, PV interneurons were genetically labeled (to prevent identification biases due to the state- and subpopulation-specific variations in PV expression; Donato et al. 2013) by injecting PV-Cre mice with an inhPSAM (tagged with GFP) or actPSAM (tagged with BTX binding site) viruses (Supplementary Fig. 4A). One month after injection, we verified by double immunostaining for PV and for the corresponding tag (GFP or BTX) that 92% of PV<sup>+</sup> neurons were GFP<sup>+</sup> (or BTX<sup>+</sup>) and that 100% of GFP<sup>+</sup> (or BTX<sup>+</sup>) neurons were PV<sup>+</sup>, confirming the precise targeting of the PV population (Supplementary Fig. 4B). We verified that, at the 3 h time point and in correspondence of the injury site, PV<sup>+</sup> cells displayed significantly higher levels of the neuronal activity marker (Knight et al., 2012) phosphorylated-S6 (pS6; median fluorescence intensity: 1340, interquartile range 1215–2015 in sal-TBI vs. 679 with an interquartile range 615–796 in sal-S,  $P < 0.0001$ ) compared with sham-operated mice (Supplementary Fig. 5A,B). Likewise, the number of c-Fos<sup>+</sup> PV interneurons was significantly higher in TBI mice than in sham mice ( $18 \pm 3$  cells/ $2.2 \times 10^5$  μm<sup>2</sup> in sal-TBI vs.  $7 \pm 2$  cells/ $2.2 \times 10^5$  μm<sup>2</sup> in sal-S,  $P < 0.0001$ ; Supplementary Fig. 5D,F), suggesting the recruitment of these interneurons by the cortical trauma. Recruitment of PV interneurons did not differ, in terms of median pS6 and in the number of c-Fos<sup>+</sup> cells, from that of non-PV neurons: in non-PV neurons, TBI induced a similar increase in pS6 (median fluorescence intensity 1483, interquartile range of 1108–1997 in sal-TBI versus 756 with an interquartile range 652–1021 in sal-S,  $P < 0.0001$ ; Supplementary Fig. 5A,C) as well as in the fraction of c-Fos<sup>+</sup> neurons (for non-PV neurons,  $18 \pm 3$  cells/ $2.2 \times 10^5$  μm<sup>2</sup> in sal-TBI vs.  $57 \pm 5$  cells/ $2.2 \times 10^5$  μm<sup>2</sup> in sal-S,  $P < 0.0001$ ; Supplementary Fig. 5E,F). Likewise, the increase in c-Fos<sup>+</sup> cells in TBI versus sham

was  $257 \pm 22\%$  in PV neurons and  $311 \pm 32\%$  in non-PV neurons ( $P=0.34$ ).

We then functionally explored the impact of PV interneurons on the biological response of principal neurons to TBI. To this end, we used PSAM/PSEM chemogenetics (Magnus et al., 2011) to either activate or inhibit PV interneurons at the time of TBI. Thereafter, we monitored the impact of activation or inhibition of PV interneurons on the acute response of cortical neurons to TBI. More specifically, PV-Cre mice were injected (30 days before the TBI) with AAV mediating either actPSAM or inhPSAM expression; 30 min before the procedure, mice were administered either the PSEM agonist (or saline) and then underwent either TBI (act-TBI, inh-TBI, or sal-TBI, respectively) or sham surgery (act-S, inh-S, and sal-S), respectively (Supplementary Figs 1A and 2A). We focused on three readouts: the levels of the activity marker pS6, the induction of c-Fos and the level of the autophagy marker LC3A in the overall neuronal (NeuN<sup>+</sup>) population (composed largely of principal neurons, Supplementary Fig. 6A–F) 3 h post-TBI.

One-way ANOVA revealed a significant difference among the groups in pS6 levels ( $F_{(5,3318)} = 209$ ,  $P < 0.0001$ ). The number of neurons counted in each case were as follows: sal-S=451, inh-S=427, act-S=495, sal-TBI=1276, inh-TBI=798, and act-TBI=822. In sham-treated mice, chemogenetic activation of PV interneurons resulted in the anticipated decrease of pS6 levels (median fluorescence intensity of 702 with an interquartile range of 480–1041 in act-S mice compared with a median fluorescence intensity of 925.9 with an interquartile range of 682–1345 in sal-S mice,  $P < 0.01$ ; Fig. 1A,B), whereas, PV inactivation caused the predicted increase in pS6 levels (median fluorescence intensity of 1105 with an interquartile range of 887–1546 in inh-S mice compared with a median fluorescence intensity of 926 with an interquartile range of 682–1345 sal-S mice,  $P < 0.01$ ; Fig. 1A,B), confirming the proper functioning of the chemogenetic system. In TBI-treated mice, a significant increase in pS6 levels in cortical neurons subjected to sal-TBI compared with sal-S was observed (median fluorescence intensity of 1565 with an interquartile range of 1209–1976 in sal-TBI mice compared with a median fluorescence intensity of 926 with an interquartile range of 682–1345 sal-S mice,  $P < 0.0001$ ; Fig. 1A,B). Interestingly, the TBI-evoked upregulation of pS6 was strongly modulated by PV interneurons: inactivation of PV interneurons (by inhPSAM/PSEM) resulted in a further increase in pS6 levels (median fluorescence intensity of 1839 with an interquartile range of 1509–2458 in inh-TBI mice compared with a median fluorescence intensity of 1564.7 with an interquartile range of 1209–1976 in sal-TBI mice,  $P < 0.0001$ ). Notably, chemogenetic activation of PV interneurons caused a massive decrease in TBI-induced pS6 upregulation (median fluorescence intensity of 969 with an interquartile range of 764–1321 in act-TBI mice compared with a median fluorescence intensity of 1565 with an interquartile range of 1209–1976 in sal-TBI mice,  $P < 0.0001$ ; Fig. 1A,B).

To confirm the changes in neuronal activation detected using pS6 immunohistochemistry, we evaluated the expression of the activity-dependent immediate-early gene c-Fos. In sham mice, once again the number of c-Fos<sup>+</sup> neurons were increased by PV inactivation and decreased by PV activation, as anticipated (inh-S vs. sal-S,  $P < 0.05$  and act-S vs. sal-S,  $P < 0.01$ ). At 3 h postinjury, sal-TBI mice showed a strong increase in c-Fos<sup>+</sup> neurons in the affected cortex ( $F_{(5,53)}=111$ ,  $P < 0.0001$ ,  $35 \pm 5$  cells/ $2.2 \times 10^5 \mu\text{m}^2$  in sal-S vs.  $101 \pm 12$  cells/ $2.2 \times 10^5 \mu\text{m}^2$  in sal-TBI mice;  $P < 0.0001$ , Fig. 1C,D), in agreement with previous reports (Chandrasekar et al. 2018). Activation of PV

interneurons at the time of trauma caused a massive decrease in c-Fos<sup>+</sup> cells 3 h after injury ( $55 \pm 6$  cells/ $2.2 \times 10^5 \mu\text{m}^2$  in act-TBI,  $P < 0.0001$  vs. sal-TBI; Fig. 1C,D) down to baseline values ( $P > 0.05$  vs. sal-S; Fig. 1C,D). On the other hand, inactivation of PV interneuron by inhPSAM significantly increased the number of c-Fos<sup>+</sup> neurons after TBI ( $129 \pm 22$  cells/ $2.2 \times 10^5 \mu\text{m}^2$  in inh-TBI vs. sal-TBI,  $P < 0.0001$ ; Fig. 1C,D).

Finally, we investigated the impact of activation/inhibition of PV interneurons on the autophagy level in principal neurons by measuring the accumulation of LC3A<sup>+</sup> aggregates. At 3 h postinjury there was a significant difference in LC3A levels for the different groups ( $F_{(5,2765)}=283$ ,  $P < 0.0001$ ). In sham mice, chemogenetic activation or inactivation of PV interneurons did not affect LC3A burden (median fluorescence intensity of 740 with an interquartile range of 548–880 in inh-S mice compared with a median fluorescence intensity of 725 with an interquartile range of 578–870 in sal-S mice,  $P > 0.05$ ; and median fluorescence intensity of 675 with an interquartile range of 546–860 in act-S mice compared with a median fluorescence intensity of 725 with an interquartile range of 578–870 in sal-S mice; Fig. 1E,F). Importantly, in saline-treated mice, TBI resulted in the significant elevation of LC3A levels in a population of principal neurons as compared with sal-S controls (median fluorescence intensity of 1250 with an interquartile range of 1024–1579 in sal-TBI;  $P < 0.0001$  vs. sal-sham; Fig. 1E,F). Interestingly, inactivation of PV interneurons strongly downregulated LC3A induction (median fluorescence intensity of 693 with an interquartile range of 461–931 in inh-TBI mice;  $P < 0.0001$  vs. sal-TBI; Fig. 1E,F) whereas stimulation of PV firing did not result in a further elevation of LC3A levels (median fluorescence intensity of 1296 with an interquartile range of 1118–1546 in act-TBI mice,  $P > 0.05$  vs. sal-TBI; Fig. 1E,F).

Notably, virtually all cells (>95%) displaying the elevation of pS6 and LC3A levels or positive for c-Fos were also NeuN<sup>+</sup>, implying that the observed responses are specifically occurring in neurons (Supplementary Fig. 5A–F).

Taken together, these findings show that PV interneurons strongly modulate neuronal activity in acute TBI and significantly affect proteostasis in principal neurons after trauma.

### Activity of PV Interneurons Modulate Neuronal Survival and Gliotic Reaction in TBI

We then investigated if the effects of PV firing at the time of TBI resulted in long-term effects on neuronal vulnerability and survival. To this end, we measured the density of NeuN<sup>+</sup> cells at 7 dpi both in the core and in the penumbra of the TBI-induced lesion (as compared with sham-operated mice). The core and penumbra were defined as depicted in Supplementary Fig. 3A. Differences between the groups (Supplementary Fig. 2B) were noted both in the core ( $F_{(5,53)}=10.05$ ,  $P < 0.0001$ ) and in the penumbra ( $F_{(5,53)}=225$ ,  $P < 0.0001$ ). No effect on NeuN<sup>+</sup> density was observed after PV activation or inactivation in mice undergoing sham surgery (core:  $29 \pm 2$ ,  $29 \pm 1$ , and  $27 \pm 1$  NeuN<sup>+</sup> cells/ $10^4 \mu\text{m}^2$  in sal-S, inh-S, and act-S, respectively,  $P > 0.05$ ; Fig. 2A; penumbra:  $32 \pm 3$ ,  $29 \pm 2$ , and  $29 \pm 2$  NeuN<sup>+</sup> cells/ $10^4 \mu\text{m}^2$  in sal-S, inh-S, and act-S, respectively,  $P > 0.05$ ). In saline-pretreated mice, irrespective of the PSAM expression, TBI resulted in an almost complete loss of NeuN<sup>+</sup> cells in the lesion core ( $2 \pm 1$  NeuN<sup>+</sup> cells/ $10^4 \mu\text{m}^2$  in sal-TBI,  $P < 0.0001$  vs. sal-S; Fig. 2A–C) and a significant cell loss in the penumbral ROI ( $14 \pm 1$  NeuN<sup>+</sup> cells/ $10^4 \mu\text{m}^2$  vs.  $29 \pm 2$  in sal-S  $P < 0.0001$ ; Fig. 2A–C). Activation of PV firing at the time of TBI did not significantly affect the number of NeuN<sup>+</sup> cells in the core ( $1 \pm 0.3$  NeuN<sup>+</sup> cells/ $10^4 \mu\text{m}^2$

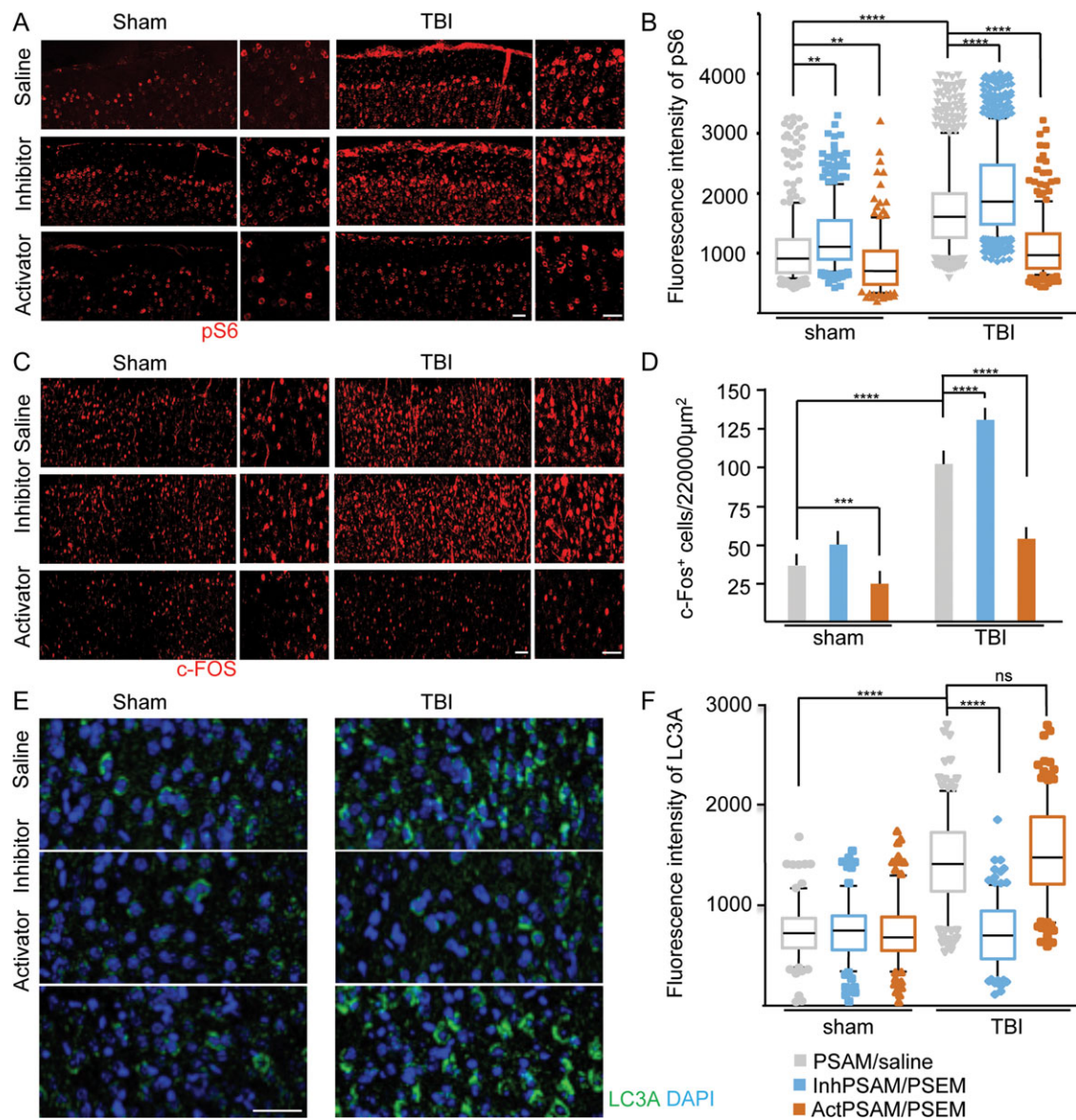


**Figure 1.** PV interneurons modulate the activity of principal neurons in TBI. (A,B) TBI triggers a strong elevation in the intensity of pS6 expression in sal-TBI mice at 3 h ( $P < 0.0001$  vs. sal-S). Suppression of PV interneuron firing by expression of the inhibitory PSAM (inh-TBI) together with PSEM administration further increases the intensity of pS6 expression in neurons after trauma ( $P < 0.0001$  vs. sal-TBI, high magnification inset) whereas activation of PV interneurons (act-TBI) massively suppresses the induction of pS6 expression in neurons after TBI ( $P < 0.0001$  vs. sal-TBI). Low magnification-Scalebar 50  $\mu\text{m}$ , high magnification inset-Scalebar 50  $\mu\text{m}$ . (C,D) Neuronal activity as detected by c-Fos expression in principal neurons is strongly increased at the injury site 3 h after TBI ( $P < 0.0001$  vs. sal-S, high magnification). Inhibiting PV interneurons further increases the number of neurons expressing c-Fos ( $P < 0.0001$  vs. sal-TBI) and activating PV interneurons has the opposite effect ( $P < 0.0001$  vs. sal-TBI). Low magnification-Scalebar 50  $\mu\text{m}$ , high magnification inset-Scalebar 50  $\mu\text{m}$ . (E,F) Autophagy is induced after TBI as seen in the elevation of LC3A expression at 3 h post-injury ( $P < 0.0001$  in sal-TBI vs. sal-S). Whereas inhibition of PV interneurons significantly downregulated expression of LC3A ( $P < 0.0001$  vs. sal-TBI), activating PV interneurons was associated with an expression of LC3A comparable to sal-TBI ( $P > 0.05$  vs. sal-TBI). Scalebar 50  $\mu\text{m}$ . \* $P < 0.05$ , \*\* $P < 0.01$ , \*\*\*\* $P < 0.0001$ .

in act-TBI vs. sal-TBI,  $P > 0.05$ ; Fig. 2A–C) but, surprisingly, it caused a significant worsening of neuronal loss in the penumbra ( $11 \pm 1$  NeuN<sup>+</sup> cells/ $10^4 \mu\text{m}^2$ ;  $P=0.005$  in act-TBI vs. sal-TBI; Fig. 2A–C). Conversely, the inactivation of PV interneurons at the time of trauma resulted in improved long-term (7 dpi) preservation of NeuN<sup>+</sup> cells in the core ( $8 \pm 1$  NeuN<sup>+</sup> cells/ $10^4 \mu\text{m}^2$  in inh-TBI,  $P < 0.0001$  vs. sal-TBI; Fig. 2A–C) as well as in the penumbra ( $22 \pm 1$  NeuN<sup>+</sup> cells/ $10^4 \mu\text{m}^2$  in inh-TBI;  $P < 0.0001$  vs. sal-TBI; Fig. 2A–C).

We assessed the effect of acute PV activation/inactivation on astrogliosis, as an independent measure of tissue damage, by monitoring the extent of GFAP immunostaining at 7 dpi. We

found significant differences in the expression of GFAP between the groups ( $F_{(5,54)}=257$ ,  $P<0.001$ ). Neither activation nor inactivation of PV interneurons affected GFAP<sup>+</sup> astrocytes in sham-surgery mice (i.e., in act-S or inh-S mice, which were comparable to sal-S). However, in mice administered with saline and subject to TBI, a significant increase in the surface area occupied by GFAP<sup>+</sup> cells were detected in the injury site (ROI area= $6.3 \times 10^4 \mu\text{m}^2$ ,  $31 \pm 1\%$  of the total area in sal-TBI vs.  $5 \pm 0.4\%$  in sal-S,  $P < 0.0001$ ; Fig. 2D, E). Notably, inactivating PV interneurons firing at the time of trauma resulted in a significantly lesser area occupied by GFAP<sup>+</sup> cells in the injury site at 7 dpi ( $9 \pm 0.5\%$  in inh-TBI,  $P < 0.0001$  vs. sal-TBI and  $P > 0.05$  vs. sal-S; Fig. 2D,E). Conversely, activation of

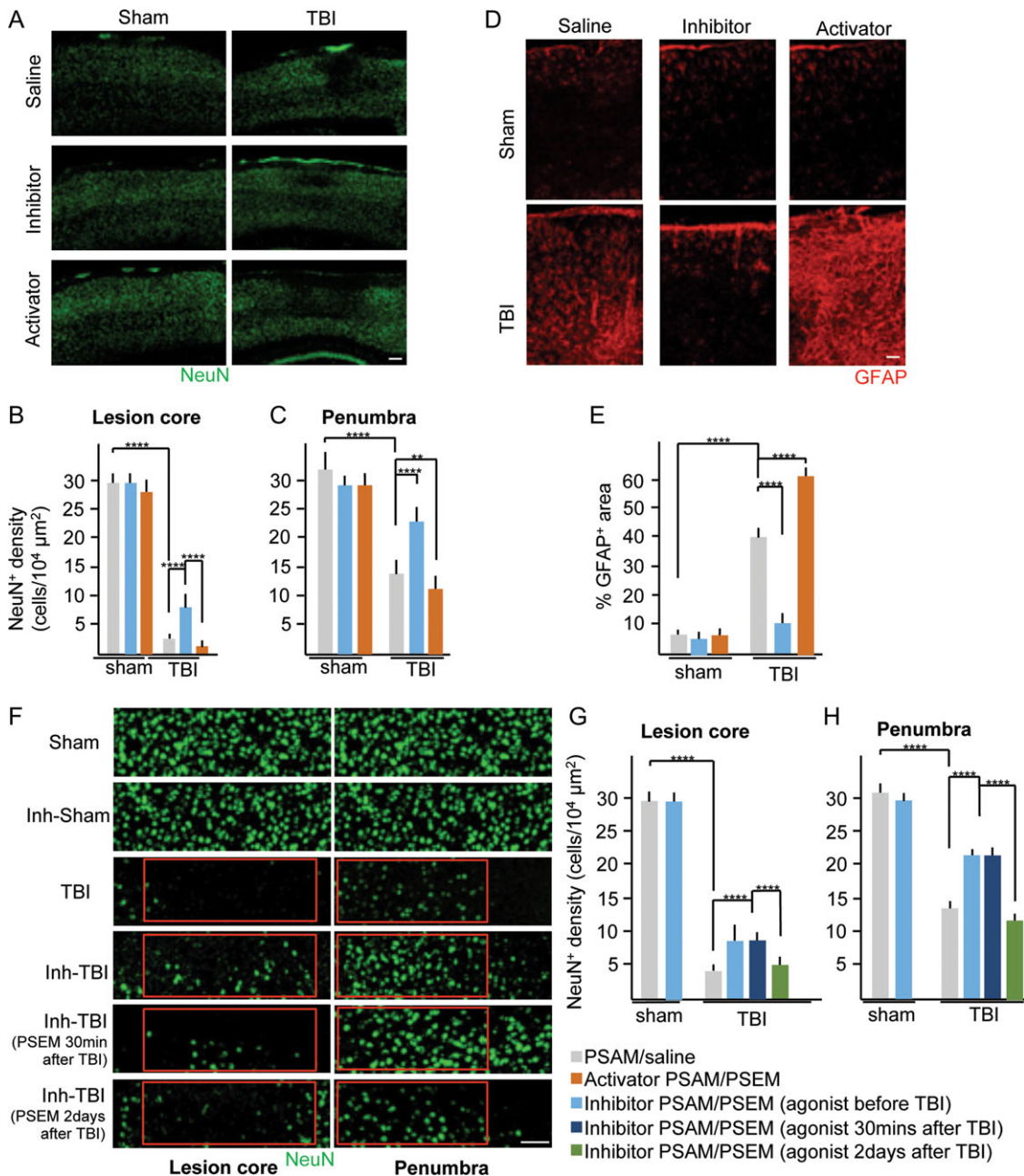


**Figure 2.** Inhibition of PV interneurons prevents neuronal death and reduces neuroinflammation. (A,B) Saline-pretreated mice display a significant loss of neurons in the core of the injury ( $P < 0.0001$  vs. sal-S). Inhibition of PV interneurons (inh-TBI) rescues a significant number of neurons in the core ( $P < 0.0001$ ), whereas activating PV interneurons (act-TBI) results in neuron loss comparable to that seen in the sal-TBI mice ( $P > 0.05$  vs. sal-TBI). Scalebar 100  $\mu\text{m}$ . (A,C) Sal-TBI mice also display a significant loss of neurons in the penumbra compared with sal-S mice ( $P < 0.0001$  vs. sal-S). The neurons in the penumbra are preserved by inhibition of PV interneurons (inh-TBI), however, leads to a greater loss of neurons as seen in sal-TBI mice ( $P < 0.001$ ). (D,E) Neuroinflammation, as shown by the astrocyte marker GFAP, was higher in sal-TBI than sal-S mice ( $P < 0.0001$ ). The neuroinflammation was reduced when PV interneurons were inhibited (inh-TBI) and comparable to sham ( $P < 0.0001$  vs. sal-TBI,  $P > 0.05$  vs. sal-S). Activating PV interneurons (act-TBI) caused a significant increase in neuroinflammation compared with sal-TBI ( $P < 0.0001$ ). Scalebar 50  $\mu\text{m}$ . (F-H) Inhibiting PV interneurons 30 min after TBI recapitulated the effect of inhibiting PV interneurons just before TBI both in the core and in the penumbra ( $P > 0.05$  vs. inh-TBI). Inhibiting PV interneurons 2 days after injury promoted neuronal survival neither in the core nor in the penumbra and was comparable to sal-TBI ( $P > 0.05$  vs. sal-TBI). Scalebar 20  $\mu\text{m}$ . \* $P < 0.05$ , \*\* $P < 0.01$ , \*\*\*\* $P < 0.0001$ .

PV interneurons resulted in a significant increase in the GFAP<sup>+</sup> volume when compared with sal-TBI ( $65 \pm 2\%$  in act-TBI,  $P < 0.0001$  vs. sal-TBI; Fig. 2D,E).

Thus, these results show that acute manipulation of PV interneurons at the time of trauma determine the extent of neuronal loss and astrogliosis caused by blunt TBI. Since we had inactivated PV interneurons at the time of trauma, we

investigated further the time constraints of the neuroprotective role of PV interneurons by inactivating them with PSEM injections administered at different time points (Supplementary Fig. 1B, refer to the methods section) relative to TBI: 30 min before TBI (acute-pre), 30 min and 8 h after TBI (acute-post), or 48 h to 96 h after TBI (subacute). The density of NeuN<sup>+</sup> neurons was assessed at 7 dpi.

At 7 dpi, significant differences were seen in NeuN<sup>+</sup> cell density among the groups (Supplementary Fig. 2C) both in the core ( $F_{(5,52)} = 851$ ,  $P < 0.0001$ ; Fig. 2F) and the penumbra ( $F_{(5,52)} = 254$ ,  $P < 0.0001$ ; Fig. 2F). As mentioned before, inhibition of PV interneurons per se (i.e., without trauma) affected neuronal vulnerability neither in the core nor the penumbra. Interestingly, inactivation of PV interneurons starting 30 min after TBI for 24 h still had a protective effect comparable to pre-TBI PV inactivation; reduced neuronal loss was observed in the injured cortex both in the core ( $8 \pm 0.6$  NeuN<sup>+</sup> cells/ $10^4 \mu\text{m}^2$  in inh-24 h-TBI vs.  $3 \pm 1$  NeuN<sup>+</sup> cells/ $10^4 \mu\text{m}^2$  in sal-TBI,  $P < 0.0001$ ,  $P > 0.05$  vs. inh-TBI; Fig. 2F-H) and the penumbra ( $22 \pm 2$  NeuN<sup>+</sup> cells/ $10^4 \mu\text{m}^2$  in inh-24 h-TBI vs.  $14 \pm 2$  NeuN<sup>+</sup> cells/ $10^4 \mu\text{m}^2$  in sal-TBI,  $P < 0.0001$ ,  $P > 0.05$  vs. inh-TBI; Fig. 2F-H). On the other hand, inactivation of PV interneurons starting 48 h after TBI could not recapitulate the protective effects of acute inactivation; inactivation of PV interneurons starting 48 h after TBI resulted in levels of neuronal loss comparable to that observed in saline-treated TBI mice both in the core ( $4 \pm 1$  NeuN<sup>+</sup> cells/ $10^4 \mu\text{m}^2$  in inh-72 h-TBI vs.  $3 \pm 1$  NeuN<sup>+</sup> cells/ $10^4 \mu\text{m}^2$  in sal-TBI,  $P > 0.05$ ,  $P < 0.0001$  vs. inh-TBI; Fig. 2F-H) and in the penumbra ( $12 \pm 1$  NeuN<sup>+</sup> cells/ $10^4 \mu\text{m}^2$  in inh-72 h-TBI vs.  $14 \pm 2$  NeuN<sup>+</sup> cells/ $10^4 \mu\text{m}^2$  in sal-TBI,  $P > 0.05$ ,  $P < 0.0001$  vs. inh-TBI; Fig. 2F-H).

Taken together, these data show that acute inactivation of PV interneurons before or soon after TBI is sufficient to enhance long-term neuronal survival and reduce astrogliosis.

### Pre-injury Ablation of PV Interneurons Increases Vulnerability of Principal Neurons to TBI

Short-term chemogenetic inhibition of PV interneurons results in a protective effect on neuronal survival in the penumbra of the injured cortex. To explore the effects of chronic loss of PV-mediated inhibition, we injected PV-Cre mice (at P30) with AAV2s encoding GFP (as a control) or a mutant Caspase-3 whose activation is controlled by the co-expression of Tobacco envelop virus protease (TEV) in Cre<sup>+</sup> cells, mutant Caspase-3 is expressed, and activated by TEV, leading to the apoptosis of the infected cell (as reported by Yang et al. 2013). We verified at P60 that the ablation strategy displayed a 97% efficiency within the infected cortical area (in an area of  $2.7 \times 10^6 \mu\text{m}^2$ , ablated mice had  $2 \pm 1$  PV<sup>+</sup> neurons compared with nonablated mice, which had  $90 \pm 5$  PV<sup>+</sup> neurons,  $P < 0.0001$ ), while nearby areas exhibited normal numbers of PV<sup>+</sup> neurons (Fig. 3A,B).

When the density of NeuN<sup>+</sup> cells were assessed at 7 dpi, a significant difference in the number of NeuN<sup>+</sup> cells among groups (Supplementary Fig. 2D) was detected both in the core ( $F_{(3,27)} = 2116$ ,  $P < 0.0001$ ) and the penumbra ( $F_{(3,27)} = 224$ ,  $P < 0.0001$ ). In abl-S mice, the loss of PV interneurons did not lead to a major loss of NeuN<sup>+</sup> cells (PV interneurons constitute only a small fraction of the total cortical neuronal population) compared with GFP-S mice ( $26.4 \pm 1.0$  NeuN<sup>+</sup> cells/ $10^4 \mu\text{m}^2$  in GFP-S vs.  $26 \pm 1$  NeuN<sup>+</sup> cells/ $10^4 \mu\text{m}^2$  in abl-S,  $P > 0.05$ ). Upon TBI, both GFP-TBI and abl-TBI mice displayed a significant loss of NeuN<sup>+</sup> cells in the core of the injury ( $3 \pm 0.7$  NeuN<sup>+</sup> cells/ $10^4 \mu\text{m}^2$  in GFP-TBI vs.  $26 \pm 1$  NeuN<sup>+</sup> cells/ $10^4 \mu\text{m}^2$  in GFP-S,  $P < 0.0001$ , and  $1 \pm 0.2$  NeuN<sup>+</sup> cells/ $10^4 \mu\text{m}^2$  in abl-TBI vs.  $26 \pm 1$  NeuN<sup>+</sup> cells/ $10^4 \mu\text{m}^2$  in abl-S,  $P < 0.0001$ , Fig. 3C,D). This loss was, however, more extensive in the ablated group ( $3 \pm 1$  NeuN<sup>+</sup> cells/ $10^4 \mu\text{m}^2$  in GFP-TBI vs.  $0.6 \pm 0.2$  NeuN<sup>+</sup> cells/ $10^4 \mu\text{m}^2$  in abl-TBI,  $P < 0.0001$ , Fig. 3C,D). Furthermore, in the penumbral area, abl-TBI mice showed a much larger loss of neurons ( $15 \pm 1$  NeuN<sup>+</sup> cells/ $10^4 \mu\text{m}^2$  in GFP-TBI vs.  $10 \pm 1$  NeuN<sup>+</sup> cells/ $10^4 \mu\text{m}^2$  in abl-TBI,  $P < 0.0001$ , as compared with  $32 \pm 1$

NeuN<sup>+</sup> cells/ $10^4 \mu\text{m}^2$  in GFP-S and  $30 \pm 4$  NeuN<sup>+</sup> cells/ $10^4 \mu\text{m}^2$  in abl-S; Fig. 3C,E).

We also examined the effects of PV interneuron ablation on the astrocytic response. In addition to the enhanced vulnerability of neurons upon chronic PV ablation, a significant difference in GFAP<sup>+</sup> area was detected ( $F_{(5,47)}=182$ ,  $P < 0.0001$ ). The glial response was significantly larger in the abl-TBI than in the gfp-TBI mice (ROI= $6.3 \times 10^4 \mu\text{m}^2$ ,  $52 \pm 2\%$  of the total area in abl-TBI vs.  $35 \pm 1\%$  in GFP-TBI,  $P < 0.0001$ ; Fig. 3F,G). The GFAP<sup>+</sup> areas in both the TBI conditions were significantly larger than in their respective sham controls ( $P < 0.0001$ ).

Taken together, these data imply that, although short-term inhibition of PV interneurons may be beneficial, their chronic ablation strongly increases the vulnerability of principal neurons to TBI.

### The Effect of Acute PV Inactivation is Mediated by Nuclear Ca<sup>2+</sup> Signals in Principal Neurons

Acute inactivation of inhibitory (PV<sup>+</sup>) interneurons delivers significant neuroprotection in both the core and the penumbra of the TBI site (Fig. 2). Since PV inactivation resulted in an increase in the activity-dependent markers c-Fos and pS6, we investigated if the neuroprotective effect was dependent on activity-regulated neuroprotective programs (Bading 2013). We reasoned that if nuclear Ca<sup>2+</sup> signals were required for PV inactivation-associated neuroprotection, neurons expressing exogenous PV-NLS would show no enhanced survival upon PSEM-mediated inactivation of PV neurons. Therefore, we co-injected mice with inhPSAM and an AAV2 driving the neuronal expression of PV-NLS-mCherry (Schlumm et al. 2013) to buffer nuclear Ca<sup>2+</sup> and prevent the induction of neuroprotective transcriptional responses (Zhang et al. 2009; Fig. 4B).

Expression of hSyn-PV-NLS-mCherry alone or together with the inhPSAM did not affect neuronal survival in sham-operated mice (not shown). One-way ANOVA revealed a significant difference in the number of PV-NLS-mCherry<sup>+</sup> cells among the different groups (Supplementary Fig. 2E) both in the core ( $F_{(2,39)}=832$ ,  $P < 0.0001$ ) and in the penumbra ( $F_{(2,39)}=23$ ,  $P < 0.0001$ ). In fact, mice expressing inhPSAM and PV-NLS-mCherry and administered with PSEM (PV inactivation and nuclear Ca<sup>2+</sup> buffering) displayed a loss of PV-NLS-mCherry<sup>+</sup> neurons comparable to mice in which PV interneurons were not inhibited (expressing the inhPSAM but administered with saline). More specifically, in the core, there were  $20 \pm 1$  PV-NLS-mCherry<sup>+</sup> cells/ $10^4 \mu\text{m}^2$  in the sham mice. For those animals receiving TBI, there were  $2 \pm 0.5$  PV-NLS-mCherry<sup>+</sup> cells/ $10^4 \mu\text{m}^2$  in NLS-inh-sal-TBI versus  $2 \pm 0.4$  PV-NLS-mCherry<sup>+</sup> cells/ $10^4 \mu\text{m}^2$  in NLS-inh-PSEM-TBI ( $P > 0.05$ ;  $P < 0.0001$  vs. NLS-inh-sal-S; Fig. 4A,C). Likewise, the penumbra of the mice injected with the PV-NLS along with the inhPSAM also showed increased vulnerability to loss of neurons ( $12 \pm 1$  PV-NLS-mCherry<sup>+</sup> cells/ $10^4 \mu\text{m}^2$  in NLS-inh-sal-TBI vs.  $18 \pm 2$  PV-NLS-mCherry<sup>+</sup> cells/ $10^4 \mu\text{m}^2$  in NLS-inh-sal-S,  $P < 0.0001$  and  $13 \pm 2$  PV-NLS-mCherry<sup>+</sup> cells/ $10^4 \mu\text{m}^2$  in NLS-inh-PSEM-TBI,  $P > 0.05$  vs. NLS-inh-sal-TBI; Fig. 4A,D). Of note, the number of PV-NLS-mCherry<sup>+</sup> cells in a third ROI (located further away from the core and not affected by TBI, Supplementary Fig. 3B) was comparable in sham and TBI samples ( $8 \pm 2$  PV-NLS-mCherry<sup>+</sup> cells/ $10^4 \mu\text{m}^2$  in NLS-inh-sal-TBI vs.  $10 \pm 2$  PV-NLS-mCherry<sup>+</sup> cells/ $10^4 \mu\text{m}^2$  in NLS-inh-sal-S,  $P < 0.0001$  and  $9 \pm 1$  PV-NLS-mCherry<sup>+</sup> cells/ $10^4 \mu\text{m}^2$  in NLS-inh-PSEM-TBI,  $P > 0.05$  vs. NLS-inh-sal-TBI and NLS-inh-sal-S; Fig. 4E), indicating a comparable infection rate in all mice. In addition, the density of inhPSAM<sup>+</sup> PV interneurons (measured in the third, not-affected



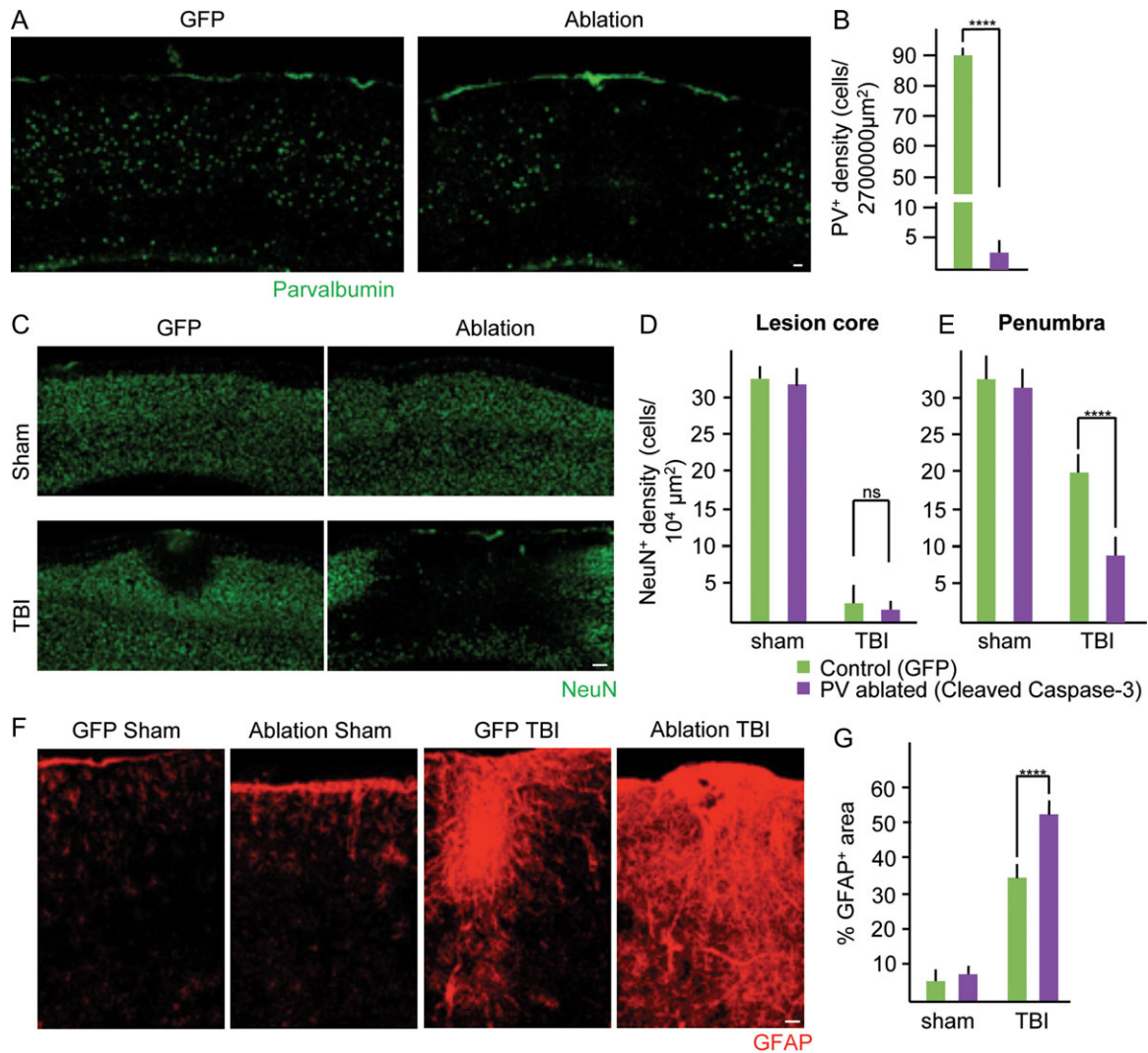


**Figure 3.** Chronic excitation of principal neurons by ablation of PV interneurons 30 days before injury could not recapitulate the effect of acute inhibition of PV interneurons before TBI. (A,B) Ablated region show a loss of almost 97% of PV interneurons when compared with mice injected with a GFP virus ( $P < 0.0001$ ). Scalebar 50  $\mu\text{m}$ . (C-E) Ablation of PV interneurons does not significantly improve neuronal survival in the lesion core over that seen in mice expressing GFP ( $P > 0.05$  vs. GFP-TBI) but resulted in a significant loss of neurons in the penumbra ( $P < 0.0001$ ). Scalebar 100  $\mu\text{m}$ . (F,G) A similar trend was seen with neuroinflammation: mice in which PV interneurons were ablated showed a significant increase in GFAP<sup>+</sup> area when compared with GFP-TBI mice ( $P < 0.0001$  vs. GFP-TBI). Scalebar 50  $\mu\text{m}$ . \* $P < 0.05$ , \*\* $P < 0.01$ , \*\*\*\* $P < 0.0001$ .

ROI) was comparable in sham and TBI mice ( $20 \pm 5$  GFP<sup>+</sup> cells/ $10^5 \mu\text{m}^2$  in NLS-inh-sal-TBI vs.  $25 \pm 7$  GFP<sup>+</sup> cells/ $10^5 \mu\text{m}^2$  in NLS-inh-sal-S,  $P > 0.05$ , and  $23 \pm 6$  GFP<sup>+</sup> cells/ $10^5 \mu\text{m}^2$  in NLS-inh-PSEM-TBI,  $P > 0.05$  vs. NLS-inh-sal-TBI and NLS-inh-sal-S, Fig. 4E), underscoring the reproducibility of the AAV injection.

Thus, the inactivation of PV interneurons enhances the survival of neurons through an activity-dependent program requiring nuclear  $\text{Ca}^{2+}$  signals.

### Direct Chemogenetic Activation of Neuronal Firing Reduces Vulnerability to TBI

Since inactivation of PV interneurons was sufficient to enhance the activation of principal neurons (Fig. 1), and provided neuroprotection following TBI through an activity-dependent neuroprotective mechanism involving nuclear  $\text{Ca}^{2+}$  signaling (Fig. 4), we explored whether a direct manipulation of principal neuron firing may mimic the effect of PV inactivation. In addition, we

explored if activity-dependent protective effect could be elicited by increasing the activity of excitatory inputs. To this end, we injected mice at P30 with an AAV8 mediating expression of the chemogenetic activator DREADD(Gq)-mCherry (under the CaMKIIa promoter) either in the side going to be subject to TBI (ipsilateral injection, Fig. 5A) or in the opposite side (contralateral injection, Fig. 5B). In the latter experiment, we aimed at exploiting the homotopic connectivity between the symmetrical somatosensory (SS) cortices (Chovsepian et al., 2017) to drive the activity of ipsilateral neurons (subject to TBI) by chemogenetically stimulating projection neurons in the contralateral cortex. Indeed, the expression of DREADD(Gq)-mCherry highlighted numerous mCherry<sup>+</sup> axons in the corpus callosum connecting the 2 hemispheres (Fig. 5B) and providing input to all layers of the SS targeted by TBI (Fig. 5A, B).

Mice subject to ipsilateral injection were administered saline or the DREADD cognate agonist, CNO (5 mg/kg), 30 min before undergoing sham surgery (Gq-sal-S or Gq-CNO-S) or TBI

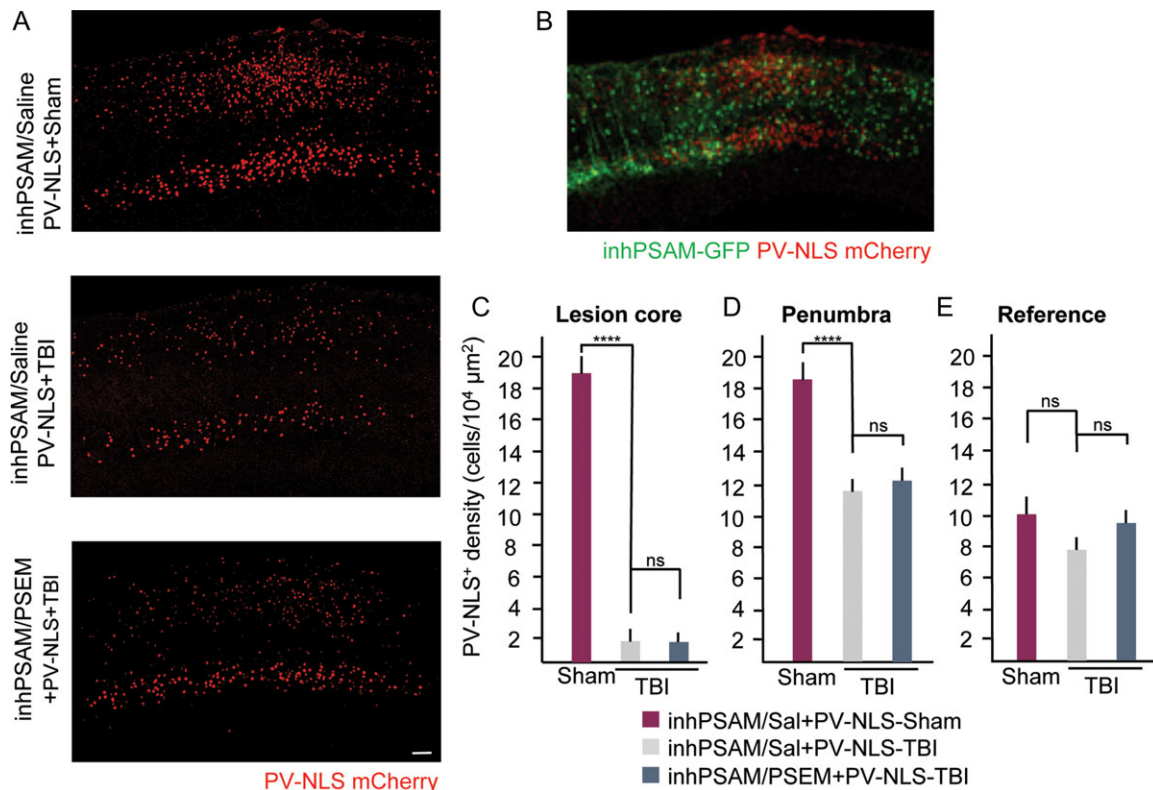


**Figure 4.** Nuclear  $\text{Ca}^{2+}$  signals in principal neurons mediate the neuroprotective effects of PV inhibition. (A,C,D) When combined with nuclear  $\text{Ca}^{2+}$  buffering, PV inhibition is unable to prevent loss of PV-NLS-mCherry<sup>+</sup> neurons both in the core ( $P > 0.05$  vs. sal-TBI) and in the penumbra ( $P > 0.05$  vs. sal-TBI). The number of PV-NLS-mCherry<sup>+</sup> neurons in the TBI conditions are much lesser than the number of PV-NLS-mCherry<sup>+</sup> neurons in the sham ( $P < 0.0001$  vs. NLS-inh-sal-S in both the core and the penumbra). Scalebar 50 μm. (B) Exogenously expressed PV-NLS-mCherry is almost exclusively observed in principal neurons at the site of injury. (E) Numbers of PV-NLS-mCherry<sup>+</sup> neurons in a third ROI (located 700 μm from the core) are similar in the sham and the TBI conditions. Scalebar 50 μm. \* $P < 0.05$ , \*\* $P < 0.01$ , \*\*\*\* $P < 0.0001$ .

(Gq-sal-TBI and Gq-CNO-TBI; Supplementary Fig. 2F). Likewise, mice subjected to contralateral injection were administered CNO before sham surgery or TBI (Gq-contra-CNO-S and Gq-contra-CNO-TBI; note that saline-treated, contralateral injected mice subject to sham surgery were equivalent to Gq-sal-S and are therefore conflated in a single group). In sham-treated mice, the excitation of ipsilateral SS by activating DREADD(Gq) resulted in a significant increase in c-Fos<sup>+</sup> cells compared with Gq-sal-S mice ( $37 \pm 5$  cells/ $2.2 \times 10^5 \mu\text{m}^2$  in Gq-sal-S vs.  $69 \pm 8$  cells/ $2.2 \times 10^5 \mu\text{m}^2$  in Gq-CNO-S,  $P < 0.001$ ). Notably, activation of the contralateral SS also resulted in a significant increase, although with a trend towards lower absolute values, in c-Fos<sup>+</sup> cells in the ipsilateral SS ( $49 \pm 7$  cells/ $2.2 \times 10^5 \mu\text{m}^2$  in Gq-contra-CNO-S vs. Gq-CNO-S,  $P = 0.2$ ; Fig. 5C,D). Thus, these results show that both ipsilateral and contralateral activation of principal neurons induce c-Fos expression. Next, we investigated the interaction between TBI and DREADD(Gq) activation on c-Fos induction. In Gq-sal-TBI mice, a significant increase in c-Fos<sup>+</sup> cells in the injured site was observed (Fig. 5D, in agreement with what shown in Fig. 1D). Notably, activation of ipsilateral DREADD(Gq) resulted in a further increase in the number of c-Fos<sup>+</sup> cells ( $104 \pm 12$  cells/ $2.2 \times 10^5 \mu\text{m}^2$  in Gq-sal-TBI vs.  $150 \pm 20$  cells/ $2.2 \times 10^5 \mu\text{m}^2$  in Gq-CNO-TBI;  $P < 0.0001$ ; Fig. 5D). On the other hand, activation of contralateral cortex resulted in a much smaller increase in the number of c-Fos<sup>+</sup> cells compared with Gq-sal-TBI ( $115 \pm 9$  cells/ $2.2 \times 10^5 \mu\text{m}^2$  in Gq-contra-CNO-TBI,  $P = 0.3827$  vs. Gq-sal-TBI, Fig. 5C,D), suggesting that the efficiency with which the contralateral cortex is activated by the injured cortex is reduced in TBI.

When neuronal preservation was assessed at 7 dpi, we found that activation of DREADD(Gq) resulted in a minor increase in neuronal preservation in the core at 7 dpi ( $3 \pm 1$  NeuN<sup>+</sup> cells/ $10^4 \mu\text{m}^2$  in Gq-CNO-TBI vs.  $1 \pm 0.4$  NeuN<sup>+</sup> cells/ $10^4 \mu\text{m}^2$  in Gq-sal-TBI,  $P < 0.0001$ ; Fig. 5E,F). However, the penumbra of the mice injected with the DREADD(Gq) showed a strong reduction in neuronal vulnerability, resulting in a pronounced preservation of neurons ( $27 \pm 3$  NeuN<sup>+</sup> cells/ $10^4 \mu\text{m}^2$  in Gq-CNO-TBI vs.  $11 \pm 1$  NeuN<sup>+</sup> cells/ $10^4 \mu\text{m}^2$  in Gq-sal-TBI,  $P < 0.0001$ ; Fig. 5E,G). Thus, direct excitation of principal neurons could recapitulate the neuroprotective effect of PV inactivation. Notably, the neuroprotective effect of direct excitation of principal neurons was comparable to the one obtained by PV inactivation ( $P = 0.24$ ; cfr. Fig. 2B,C and Fig. 5F,G).

When we investigated the effect of contralateral cortex activation on neuronal integrity at 7 dpi. One-way ANOVA revealed a significant difference of NeuN<sup>+</sup> cells between the four groups (Supplementary Fig. 2F) both in the core ( $F_{(3,32)} = 22$ ,  $P < 0.0001$ ) and in the penumbra ( $F_{(3,32)} = 83$ ,  $P < 0.0001$ ). However, in contrast to the observation when principal neurons were directly (ipsilateral) activated, activation of the contralateral cortex produced no difference in the neuronal survival in the core ( $1 \pm 0.6$  NeuN<sup>+</sup> cells/ $10^4 \mu\text{m}^2$  in Gq-sal-contra-TBI when compared with  $1 \pm 0.4$  NeuN<sup>+</sup> cells/ $10^4 \mu\text{m}^2$  in Gq-contra-CNO-TBI,  $P > 0.05$ ) and only a modest (although statistically significant) increase in the number of neurons in the penumbra of the Gq-contra-CNO-TBI mice when compared with the Gq-contra-sal-TBI was observed ( $16 \pm 3$  NeuN<sup>+</sup> cells/ $10^4 \mu\text{m}^2$  in Gq-contra-CNO-TBI,  $12 \pm 2$  NeuN<sup>+</sup> cells/ $10^4 \mu\text{m}^2$  in Gq-contra-sal-TBI when compared with  $P < 0.05$ ; Fig. 5E–G) indicating that synaptic activity may produce a small but significant neuroprotective effect.

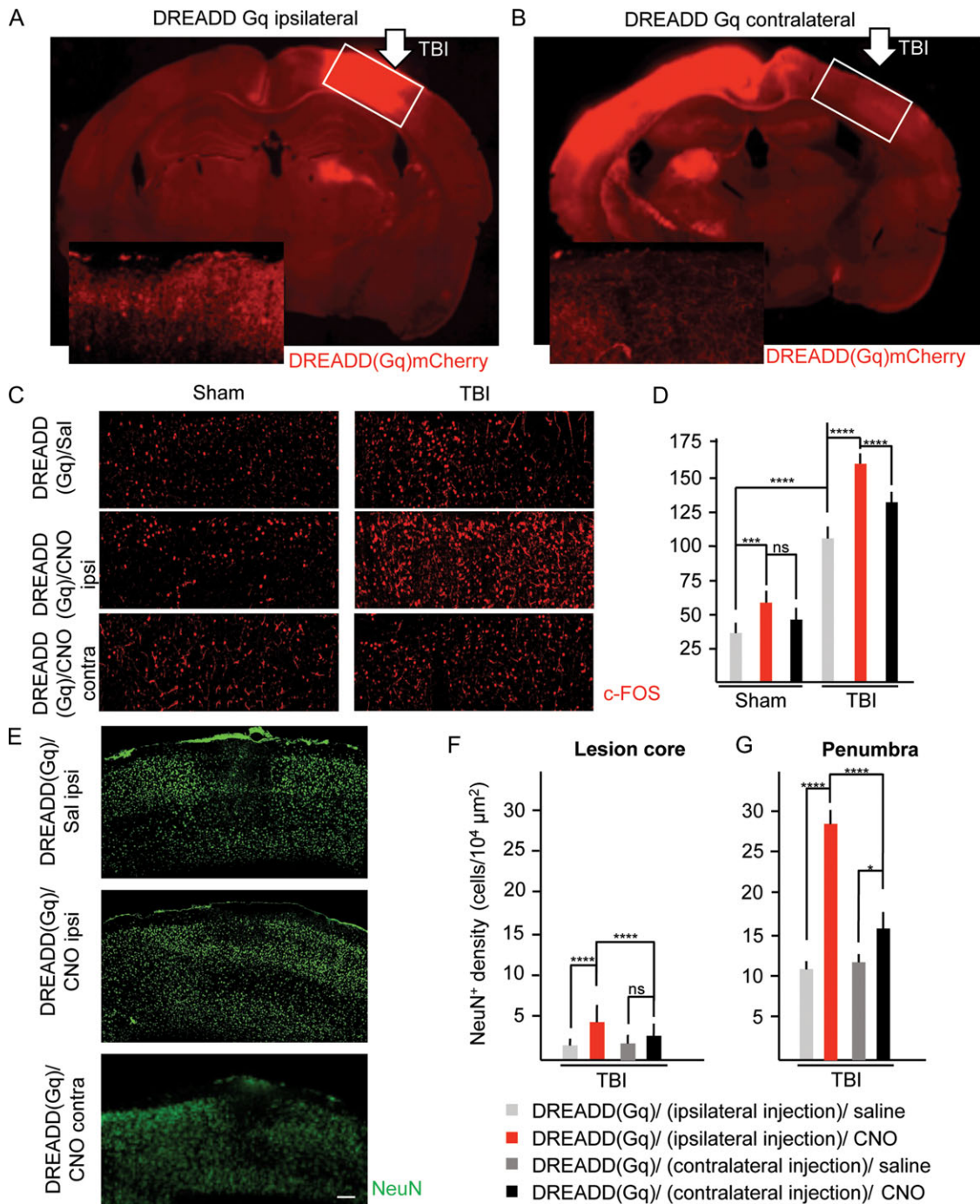


**Figure 5.** Direct excitation of principal neurons produces an effect similar to PV interneuron inhibition, but this effect is not recapitulated by indirect excitation. (A,B) Ipsilateral (A) and contralateral (B) expression of the mCherry-tagged DREADD Gq with a CaMKIIa promoter. The axons can be seen crossing the corpus callosum. The insets show the injection site in the ipsilateral injection (site of trauma) and the axons at the site of the trauma in case of the contralateral injection. Scalebar 50 μm. (C–E) Activation of principal neurons at the site of injury further increased the number of c-Fos<sup>+</sup> neurons when compared with TBI alone ( $P > 0.0001$  vs. sal-TBI). The number of c-Fos<sup>+</sup> neurons on the contralateral side was comparable to TBI ( $P > 0.05$ ). Scalebar 50 μm. (F,G) Activation of principal neurons at the site of the injury helps preserve neurons both in the core ( $P < 0.0001$  vs. sal-TBI) and the penumbra ( $P < 0.0001$  vs. sal-TBI). Indirect excitation of principal neurons (achieved by injecting the virus in the contralateral cortex) is unable to recapitulate this effect and is associated with a loss of neurons in the core similar to that seen in of sal-TBI mice ( $P > 0.05$  vs. sal-TBI) and with a very modest increase in the number of neurons in the penumbra ( $P < 0.05$  vs. sal-TBI). Scalebar 50 μm. \* $P < 0.05$ , \*\* $P < 0.01$ , \*\*\*\* $P < 0.0001$ .

These findings show that activating neurons directly at the site of the TBI helps preserve neurons both in the core as well as the penumbra, and that this effect cannot be recapitulated by indirect activation of the neurons via afferents arising from the contralateral cortex.

## Discussion

In the present work we have demonstrated that chemogenetic manipulation of cortical microcircuitry involving PV interneurons modulates neuronal loss in TBI. Acute inactivation of PV

interneurons is sufficient to decrease autophagy, enhance protein synthesis and promote the survival of principal neurons; conversely, stimulation of PV firing results in the decreased viability of principal neurons and increases gliosis. Notably, chronic depletion of PV interneurons results in the reverse effect, leading to an increase in neuronal loss. Mechanistically, we show that the beneficial effect of early PV inactivation is prevented by buffering nuclear  $\text{Ca}^{2+}$ , suggesting that an activity-regulated nuclear  $\text{Ca}^{2+}$  signal is responsible for the activity-dependent neuroprotection. Thus, we provide evidence that (i) interventions on cortical microcircuitry may modulate principal neurons vulnerability to TBI, and (ii) maintaining excitation in acute TBI may exhibit protective effects (summarized in Supplementary Fig. 7).

Interestingly, several reports have shown that spontaneous and evoked the activity in cortex appears to be suppressed in the acute phase (i.e., within a few minutes or hours) after TBI (Carron et al. 2016). In fact, 24 h after trauma, cortical responses to sensory stimuli are significantly reduced and principal neurons, particularly in the upper layers, are hypoexcitable (Johnstone et al. 2013). The suppression of stimulus-evoked cortical activity has been reported to be independent of the type of TBI model (Johnstone et al. 2014). The suppression of cortical activity seems to affect infra- and supragranular principal neurons within the first 2 weeks after TBI (Allitt et al. 2016), well before hyperexcitability can be identified in the chronic phase (8 weeks after TBI; Ding et al. 2011; Johnstone et al. 2013; Allitt et al. 2017). Notably, persistent downregulation of neuronal firing has been recorded after the occurrence of Cortical Spreading Depression (CSD), a feature often associated with TBI (Hinzman et al. 2015). A significant decrease in action potential frequency together with an increase in the size of inhibitory postsynaptic potentials has also been described, ultimately resulting in a net shift of the excitation/inhibition balance toward increased inhibition (Sawant-Pokam et al. 2017). Notably, increasing inhibition by administering GABAergic drugs increases the occurrence of CSD in human patients (Hertle et al. 2012, 2016), suggesting that excess inhibition may be detrimental in this condition.

PV interneurons are powerful modulators of cortical excitability and might exert strong effects on cortical excitability in normal as well as in pathological conditions. In fact, strong activation of PV interneurons is sufficient to completely silence cortical areas (Atallah et al. 2012) whereas inactivation of PV interneurons is sufficient to increase the basal and evoked firing rate of principal neurons in the somatosensory cortex (Agetsuma et al. 2017; Yang et al. 2017). Likewise, PV interneurons are recruited early in epileptic discharges (Cammarota et al. 2013; Khoshkhoo et al. 2017) and activation of PV interneurons can block the propagation of pathological discharges (Trevelyan et al. 2006; Paz et al. 2013). Here we have demonstrated that PV interneurons offer an entry point to controlling cortical activity in the early phases after trauma. In fact, not only are PV interneurons recruited in TBI (as shown by elevation of pS6 and c-Fos in PV<sup>+</sup> neurons), but their inactivation enhances, and their forced activation downregulates activity markers. In this way, the modulation of PV firing effectively modifies the biological response of principal neurons to TBI, decreasing the overall levels of the autophagic response. Although PV interneurons can effectively modulate the cortical response to TBI, their contribution to the cortical silencing that occurs after the trauma remains to be investigated. In this direction, we have recently found (Chandrasekar et al., unpublished data) that TBI upregulates the phosphorylation of ErbB RTK in excitatory synapses of PV interneurons, a condition associated

with increased excitation of PV interneurons (Sun et al. 2016) and an overall increase in GABAergic output (Lu et al. 2014). It is conceivable, therefore, that PV interneurons may actually be involved in the pathophysiological regulation of activity within microcircuits soon after trauma. These early events may affect principal neuronal survival at a critical junction within the first 24 h after trauma. In fact, the effectiveness of PV inactivation disappears when treatment is given in a delayed manner (from 2 dpi). Interestingly, the amount of inhibition provided by PV interneurons seem to decrease after 24 h (at least in a mild TBI trauma; Vascak et al. 2017) and progressive degeneration of PV interneurons may contribute to the chronic hyperexcitability of the injured cortex (Buritica et al. 2009; Hsieh et al. 2017; although not in all models: Carron et al. 2016). Interestingly, loss of PV interneurons has been reported even in presence of preserved number of NeuN<sup>+</sup> neurons (Hsieh et al. 2017). Thus, the link between loss of PV interneurons after TBI, appearance of chronic hyperexcitability (2–4 weeks after TBI) and long-term loss of principal neurons remains to be verified.

Although early inactivation of PV interneurons may affect acute biology after TBI and enhance overall survival of neurons, permanent ablation of PV interneurons does not prove beneficial (and may actually increase the area of neuronal loss). Thus, the chronic hyperexcitability of principal neurons that is anticipated to occur (Martin and Sloviter 2001) may enhance their vulnerability to the excitatory wave triggered by the trauma itself; on this basis, one may speculate that, although PV interneuron inactivation is beneficial after trauma, these cells may also be required for the control of acute epileptiform activity (Trevelyan et al. 2006; Khoshkhoo et al. 2017).

The neuroprotective effect of early PV inactivation can be recapitulated by direct activation of principal neurons with the unrelated DREADD(Gq) system (under the CaMKIIa promoter); in agreement with the proapoptotic effect of NMDAR antagonists in the subacute stage of TBI (Pohl et al. 1999) and with the neuroprotective effect of excitation observed in neurodegenerative conditions (Saxena et al., 2013; Roselli and Caroni, 2015), sustaining neuronal activity appears to be a viable option to deliver neuroprotection in TBI. In agreement with the limited response of cortical neurons subjected to trauma to synaptically-evoked stimulation (Johnstone et al. 2013), the degree of c-Fos expression, and the neuroprotective effect obtained through circuit activation (i.e., by activating contralateral, symmetrically-projecting projection neurons), was significantly smaller than that obtained by direct stimulation. Thus, the effects of synaptic excitation may be limited by the TBI itself (by injuring transcallosal axons and/or by increasing the activity of local PV interneurons), and therefore be unable to sustain synaptic activity-dependent neuroprotective programs.

As an underlying mechanism, we show that the long-lasting effect of acute inactivation of PV interneurons is blocked by the expression of an engineered nuclear  $\text{Ca}^{2+}$  buffer (Schlumm et al. 2013), further confirming the excitation-dependent neuroprotective pathway. Indeed, synaptic activity and excitation-dependent transcriptional responses have been shown to generate a state of “acquired neuroprotection”, which renders neurons less vulnerable to stressors while not affecting neuronal survival at baseline (Zhang et al. 2009). The build up of this “neuroprotective shield” is controlled by nuclear  $\text{Ca}^{2+}$  signaling (Bading 2013) and involves the activation of the CREB/CBP transcription factor complex, as well as the IEG transcription factors, ATF-3 and Npas4, and the secreted proteins, inhibin $\beta$ A and SerpinB2 (Zhang et al. 2009, 2011; Bading 2013; Qiu et al. 2013; Ahlgren et al. 2014). Acquired neuroprotection attenuates excitotoxicity by mechanically

distinct processes, which includes inhibin $\beta$ A-mediated reduction of toxic extrasynaptic NMDA receptor signaling (Lau et al. 2015), a shift in energy metabolism towards glycolysis (“Neuronal Warburg effect”; Bas-Orth et al. 2017), a decrease in mitochondrial  $\text{Ca}^{2+}$  load through Npas4 mediated suppression of the mitochondrial calcium uniporter (Mcu) (Qiu et al. 2013), and increased resilience to oxidative stress and oxygen radicals production (Papadia et al. 2008; Depp et al. 2017). The beneficial effects of promoting ongoing activity may affect additional readouts besides neuronal survival. For example, TBI causes acute and subacute dendritic degeneration and synaptic loss (Winston et al. 2013; Wang et al. 2016), whereas the synaptic activity- and nuclear  $\text{Ca}^{2+}$ -regulated factor, VEGF-D up-holds structural integrity of dendritic arbors (Mauceri et al. 2011), and suppression by nuclear  $\text{Ca}^{2+}$  of C1q, a synapse pruning factor (Simonetti et al. 2013) prevents spine loss (Mauceri et al. 2015).

Notably, the neuroprotective effect delivered by increasing neuronal activity, either directly or indirectly, appears to be more pronounced in the penumbra rather than in core. It is conceivable that neurons lost due to trauma physical forces or acute excitotoxicity (unfolding in seconds or minute after injury) are relatively insensitive to activity-dependent mechanisms, whereas neurons in the penumbra may be affected by pathogenic processes (taking place over hours or days), such as extrasynaptic glutamate receptor activation (Bading 2017), neuroinflammation, and oxidative stress, which may be effectively counteracted by excitation-activated transcriptional programs (Zhang et al. 2009, 2011; Depp et al. 2017; Foerstner et al. 2018).

Thus, in a condition of acute excitotoxicity, maintaining an active synaptic network may enable the surviving neurons, in the core and possibly even more in the penumbra, to access a number of protective programs. In contrast, the shut-down of neuronal activity may render the surviving neurons more vulnerable to the unfavorable conditions generated by the trauma and by TBI primary injury.

## Supplementary Material

Supplementary material is available at *Cerebral Cortex* online.

## Funding

This work has been supported by the Deutsche Forschungsgemeinschaft (DFG) as part of the Collaborative Research Center 1149 “Danger Response, Disturbance Factors and Regenerative Potential after Acute Trauma” (SFB1149-B05). H.B. is supported by the Collaborative Research Center 1158 (SFB 1158-A05). F.R. is also supported by the ERANET-NEURON initiative “External Insults to the Nervous System” and BMBF as part of the MICRONET consortium (FKZ 01EW1705A), by the Synapsis Foundation and by the Baustein program of the Medical Faculty of Ulm University.

## Notes

*Conflict of Interest:* None declared.

## References

- Agetsuma M, Hamm JP, Tao K, Fujisawa S, Yuste R. 2017. Parvalbumin-positive interneurons regulate neuronal ensembles in visual cortex. *Cereb Cortex*. 6:1–15.
- Ahlgren H, Bas-Orth C, Freitag HE, Hellwig A, Ottersen OP, Bading H. 2014. The nuclear calcium signaling target, activating transcription factor 3 (ATF3), protects against dendrotoxicity and facilitates the recovery of synaptic transmission after an excitotoxic insult. *J Biol Chem*. 289(14):9970–9982.
- Allitt BJ, Iva P, Yan EB, Rajan R. 2016. Hypo-excitation across all cortical laminae defines intermediate stages of cortical neuronal dysfunction in diffuse traumatic brain injury. *Neuroscience*. 334:290–308.
- Allitt BJ, Johnstone VPA, Richards KL, Yan EB, Rajan R. 2017. Progesterone sharpens temporal response profiles of sensory cortical neurons in animals exposed to traumatic brain injury. *Cell Transplant*. 26(7):1202–1223.
- Aschauer DF, Kreuz S, Rumpel S. 2013. Analysis of transduction efficiency, tropism and axonal transport of AAV serotypes 1, 2, 5, 6, 8 and 9 in the mouse brain. *PLoS One*. 8(9):e76310.
- Atallah BV, Bruns W, Carandini M, Scanziani M. 2012. Parvalbumin-expressing interneurons linearly transform cortical responses to visual stimuli. *Neuron*. 73(1):159–170.
- Bading H. 2013. Nuclear calcium signalling in the regulation of brain function. *Nat Rev Neurosci*. 14(9):593–608.
- Bading H. 2017. Therapeutic targeting of the pathological triad of extrasynaptic NMDA receptor signaling in neurodegenerations. *J Exp Med*. 214:569–578.
- Bas-Orth C, Tan YW, Lau D, Bading H. 2017. Synaptic activity drives a genomic program that promotes a neuronal warburg effect. *J Biol Chem*. 292(13):5183–5194.
- Buriticá E, Villamil L, Guzmán F, Escobar MI, García-Cairasco N, Pimienta HJ. 2009. Changes in calcium-binding protein expression in human cortical contusion tissue. *J Neurotrauma*. 26(12):2145–2155.
- Cammarota M, Losi G, Chiavegato A, Zonta M, Carmignoto G. 2013. Fast spiking interneuron control of seizure propagation in a cortical slice model of focal epilepsy. *J Physiol*. 591(4):807–822.
- Cantu D, Walker K, Andresen L, Taylor-Weiner A, Hampton D, Tesco G, Dulla CG. 2015. Traumatic brain injury increases cortical glutamate network activity by compromising GABAergic control. *Cereb Cortex*. 25(8):2306–2320.
- Cardin JA, Carlén M, Meletis K, Knoblich U, Zhang F, Deisseroth K, Tsai LH, Moore CI. 2009. Driving fast-spiking cells induces gamma rhythm and controls sensory responses. *Nature*. 459(7247):663–667.
- Carron SF, Alwis DS, Rajan R. 2016. Traumatic brain injury and neuronal functionality changes in sensory cortex. *Front Syst Neurosci*. 10:47.
- Chandrasekar A, Aksan B, Heuvel FO, Förstner P, Sinske D, Rehman R, Palmer A, Ludolph A, Huber-Lang M, Böckers T, et al. 2018. Neuroprotective effect of acute ethanol intoxication in TBI is associated to the hierarchical modulation of early transcriptional responses. *Exp Neurol*. 302:34–45.
- Chovepian A, Empl L, Correa D, Bareyre FM. 2017. Heterotopic transcallosal projections are present throughout the mouse cortex. *Front Cell Neurosci*. 11:36.
- Defelipe J, González-Albo MC, Del Río MR, Elston GN. 1999. Distribution and patterns of connectivity of interneurons containing calbindin, calretinin, and parvalbumin in visual areas of the occipital and temporal lobes of the macaque monkey. *J Comp Neurol*. 412(3):515–526.
- Depp C, Bas-Orth C, Schroeder L, Hellwig A, Bading H. 2017. Synaptic activity protects neurons against calcium-mediated oxidation and contraction of mitochondria during excitotoxicity. *Antioxid Redox Signal*. doi:10.1089/ars.2017.7092[Epub ahead of print].
- Dietrich WD, Alonso O, Busto R, Ginsberg MD. 1994. Widespread metabolic depression and reduced somatosensory circuit

- activation following traumatic brain injury in rats. *J Neurotrauma*. 11(6):629–640.
- Ding MC, Wang Q, Lo EH, Stanley GB. 2011. Cortical excitation and inhibition following focal traumatic brain injury. *J Neurosci*. 31(40):14085–14094.
- Donato F, Chowdhury A, Lahr M, Caroni P. 2015. Early- and late-born parvalbumin basket cell subpopulations exhibiting distinct regulation and roles in learning. *Neuron*. 85(4):770–786.
- Donato F, Rompani SB, Caroni P. 2013. Parvalbumin-expressing basket-cell network plasticity induced by experience regulates adult learning. *Nature*. 504(7479):272–276.
- Flierl MA, Stahel PF, Beauchamp KM, Morgan SJ, Smith WR, Shohami E. 2009. Mouse closed head injury model induced by a weight-drop device. *Nat Protoc*. 4:1328–1337.
- Foerstner P, Rehman R, Anastasiadou S, Haffner-Luntzer M, Sinske D, Ignatius A, Roselli F, Knoell B. 2018. Neuroinflammation after traumatic brain injury (TBI) is enhanced in activating transcription factor 3 (ATF3) mutant mice. *J Neurotrauma*. doi:10.1089/neu.2017.5593[Epub ahead of print].
- Haider B, Häusser M, Carandini M. 2013. Inhibition dominates sensory responses in the awake cortex. *Nature*. 493(7430):97–100.
- Hardingham GE, Bading H. 2010. Synaptic versus extrasynaptic NMDA receptor signalling: implications for neurodegenerative disorders. *Nat Rev Neurosci*. 11(10):682–696.
- Hardingham GE, Fukunaga Y, Bading H. 2002. Extrasynaptic NMDARs oppose synaptic NMDARs by triggering CREB shut-off and death pathways. *Nat Neurosci*. 5:405–415.
- Hertle DN, Beynon C, Neumann JO, Santos E, Sánchez-Porrás R, Unterberg AW, Sakowitz OW. 2016. Use of GABAergic sedatives after subarachnoid hemorrhage is associated with worse outcome-preliminary findings. *J Clin Anesth*. 35:118–122.
- Hertle DN, Dreier JP, Woitzik J, Hartings JA, Bullock R, Okonkwo DO, Shutter LA, Vidgeon S, Strong AJ, Kowoll C, et al. 2012. Cooperative Study of Brain Injury Depolarizations (COSBID). Effect of analgesics and sedatives on the occurrence of spreading depolarizations accompanying acute brain injury. *Brain*. 135(Pt 8):2390–2398.
- Hinzman JM, DiNapoli VA, Mahoney EJ, Gerhardt GA, Hartings JA. 2015. Spreading depolarizations mediate excitotoxicity in the development of acute cortical lesions. *Exp Neurol*. 267:243–253.
- Hsieh TH, Lee HHC, Hameed MQ, Pascual-Leone A, Hensch TK, Rotenberg A. 2017. Trajectory of parvalbumin cell impairment and loss of cortical inhibition in traumatic brain injury. *Cereb Cortex*. 27(12):5509–5524.
- Hu H, Gan J, Jonas P. 2014. Interneurons. Fast-spiking, parvalbumin<sup>+</sup> GABAergic interneurons: from cellular design to microcircuit function. *Science*. 345(6196):1255–1263.
- Isaacson JS, Scanziani M. 2011. How inhibition shapes cortical activity. *Neuron*. 72(2):231–243.
- Johnstone VP, Shultz SR, Yan EB, O'Brien TJ, Rajan R. 2014. The acute phase of mild traumatic brain injury is characterized by a distance-dependent neuronal hypoactivity. *J Neurotrauma*. 31(22):1881–1895.
- Johnstone VP, Yan EB, Alwis DS, Rajan R. 2013. Cortical hypoexcitation defines neuronal responses in the immediate aftermath of traumatic brain injury. *PLoS One*. 8(5):e63454.
- Karunakaran S, Chowdhury A, Donato F, Quairiaux C, Michel CM, Caroni P. 2016. PV plasticity sustained through D1/5 dopamine signaling required for long-term memory consolidation. *Nat Neurosci*. 19:454–464.
- Kaur P, Sharma S. 2017. Recent advances in pathophysiology of traumatic brain injury. *Curr Neuropharmacol*. doi:10.2174/1570159X15666170613083606[Epub ahead of print].
- Khoshkhoo S, Vogt D, Sohal VS. 2017. Dynamic, cell-type-specific roles for gabaergic interneurons in a mouse model of optogenetically inducible seizures. *Neuron*. 93(2):291–298.
- Knight ZA, Tan K, Birsoy K, Schmidt S, Garrison JL, Wysocki RW, Emiliano A, Ekstrand MI, Friedman JM. 2012. Molecular profiling of activated neurons by phosphorylated ribosome capture. *Cell*. 151(5):1126–1137.
- Lau D, Bengtson CP, Buchthal B, Bading H. 2015. BDNF reduces toxic extrasynaptic NMDA receptor signaling via synaptic NMDA receptors and nuclear-calcium-induced transcription of inhba/activin A. *Cell Rep*. 12(8):1353–1366.
- Lu Y, Sun XD, Hou FQ, Bi LL, Yin DM, Liu F, Chen YJ, Bean JC, Jiao HF, Liu X, et al. 2014. Maintenance of GABAergic activity by neuregulin 1-ErbB4 in amygdala for fear memory. *Neuron*. 84(4):835–846.
- Léveillé F, Papadia S, Fricker M, Bell KF, Soriano FX, Martel MA, Puddifoot C, Habel M, Wyllie DJ, Ikonomidou C, et al. 2010. Suppression of the intrinsic apoptosis pathway by synaptic activity. *J Neurosci*. 30(7):2623–2635.
- Magnus CJ, Lee PH, Atasoy D, Su HH, Looger LL, Sternson SM. 2011. Chemical and genetic engineering of selective ion channel-ligand interactions. *Science*. 333:1292–1296.
- Martin JL, Sloviter RS. 2001. Focal inhibitory interneuron loss and principal cell hyperexcitability in the rat hippocampus after microinjection of a neurotoxic conjugate of saporin and a peptidase-resistant analog of Substance P. *J Comp Neurol*. 436(2):127–152.
- Mauceri D, Freitag HE, Oliveira AM, Bengtson CP, Bading H. 2011. Nuclear calcium-VEGFD signaling controls maintenance of dendrite arborization necessary for memory formation. *Neuron*. 71:117–130.
- Mauceri D, Hagenston AM, Schramm K, Weiss U, Bading H. 2015. Nuclear calcium buffering capacity shapes neuronal architecture. *J Biol Chem*. 290(38):23039–23049.
- Papadia S, Soriano FX, Léveillé F, Martel MA, Dakin KA, Hansen HH, Kaindl A, Sifringer M, Fowler J, Stefovská V, et al. 2008. Synaptic NMDA receptor activity boosts intrinsic antioxidant defenses. *Nat Neurosci*. 11(4):476–487.
- Paz JT, Davidson TJ, Frechette ES, Delord B, Parada I, Peng K, Deisseroth K, Huguenard JR. 2013. Closed-loop optogenetic control of thalamus as a tool for interrupting seizures after cortical injury. *Nat Neurosci*. 16(1):64–70.
- Pohl D, Bittigau P, Ishimaru MJ, Stadthaus D, Hübner C, Olney JW, Turski L, Ikonomidou C. 1999. N-Methyl-D-aspartate antagonists and apoptotic cell death triggered by head trauma in developing rat brain. *Proc Natl Acad Sci U S A*. 96(5):2508–2513.
- Qiu J, Tan YW, Hagenston AM, Martel MA, Kneisel N, Skehel PA, Wyllie DJ, Bading H, Hardingham GE. 2013. Mitochondrial calcium uniporter Mcu controls excitotoxicity and is transcriptionally repressed by neuroprotective nuclear calcium signals. *Nat Commun*. 4:2034.
- Roselli F, Caroni P. 2015. From intrinsic firing properties to selective neuronal vulnerability in neurodegenerative diseases. *Neuron*. 85:901–910.
- Roth BL. 2016. DREADDs for neuroscientists. *Neuron*. 89(4):683–694.
- Samson AJ, Robertson G, Zagnoni M, Connolly CN. 2016. Neuronal networks provide rapid neuroprotection against spreading toxicity. *Sci Rep*. 6:33746.

- Sawant-Pokam PM, Suryavanshi P, Mendez JM, Dudek FE, Brennan KC. 2017. Mechanisms of neuronal silencing after cortical spreading depression. *Cereb Cortex*. 27(2):1311–1325.
- Saxena S, Roselli F, Singh K, Leptien K, Julien JP, Gros-Louis F, Caroni P. 2013. Neuroprotection through excitability and mTOR required in ALS motoneurons to delay disease and extend survival. *Neuron*. 80:80–96.
- Schlumm F, Mauceri D, Freitag HE, Bading H. 2013. Nuclear calcium signaling regulates nuclear export of a subset of class IIa histone deacetylases following synaptic activity. *J Biol Chem*. 288(12):8074–8084.
- Simonetti M, Hagenston AM, Vardeh D, Freitag HE, Mauceri D, Lu J, Satagopam VP, Schneider R, Costigan M, Bading H, et al. 2013. Nuclear calcium signaling in spinal neurons drives a genomic program required for persistent inflammatory pain. *Neuron*. 77:43–57.
- Sun D, Chen X, Gu G, Wang J, Zhang J. 2017. Potential roles of mitochondria-associated ER membranes (MAMs) in traumatic brain injury. *Cell Mol Neurobiol*. 37(8):1349–1357.
- Sun Y, Ikrar T, Davis MF, Gong N, Zheng X, Luo ZD, Lai C, Mei L, Holmes TC, Gandhi SP, et al. 2016. Neuregulin-1/ErbB4 signaling regulates visual cortical plasticity. *Neuron*. 92(1):160–173.
- Trevelyan AJ, Sussillo D, Watson BO, Yuste R. 2006. Modular propagation of epileptiform activity: evidence for an inhibitory veto in neocortex. *J Neurosci*. 26(48):12447–12455.
- Vascak M, Jin X, Jacobs KM, Povlishock JT. 2017. Mild traumatic brain injury induces structural and functional disconnection of local neocortical inhibitory networks via parvalbumin interneuron diffuse axonal injury. *Cereb Cortex*. 4:1–20.
- Wang CF, Zhao CC, Jiang G, Gu X, Feng JF, Jiang JY. 2016. The role of posttraumatic hypothermia in preventing dendrite degeneration and spine loss after severe traumatic brain injury. *Sci Rep*. 6:37063.
- Weber JT. 2012. Altered calcium signaling following traumatic brain injury. *Front Pharmacol*. 3:60.
- Wilent WB, Contreras D. 2005. Dynamics of excitation and inhibition underlying stimulus selectivity in rat somatosensory cortex. *Nat Neurosci*. 8(10):1364–1370.
- Winston CN, Chellappa D, Wilkins T, Barton DJ, Washington PM, Loane DJ, Zapple DN, Burns MP. 2013. Controlled cortical impact results in an extensive loss of dendritic spines that is not mediated by injury-induced amyloid-beta accumulation. *J Neurotrauma*. 30(23):1966–1972.
- Wroge CM, Hogins J, Eisenman L, Mennerick S. 2012. Synaptic NMDA receptors mediate hypoxic excitotoxic death. *J Neurosci*. 32(19):6732–6742.
- Yang CF, Chiang MC, Gray DC, Prabhakaran M, Alvarado M, Juntti SA, Unger EK, Wells JA, Shah NM. 2013. Sexually dimorphic neurons in the ventromedial hypothalamus govern mating in both sexes and aggression in males. *Cell*. 153(4):896–909.
- Yang JW, Prouvot PH, Reyes-Puerta V, Stüttgen MC, Stroh A, Luhmann HJ. 2017. Optogenetic modulation of a minor fraction of parvalbumin-positive interneurons specifically affects spatiotemporal dynamics of spontaneous and sensory-evoked activity in mouse somatosensory cortex *in vivo*. *Cereb Cortex*. 27(12):5784–5803.
- Zhang SJ, Buchthal B, Lau D, Hayer S, Dick O, Schwaninger M, Veltkamp R, Zou M, Weiss U, Bading H. 2011. A signaling cascade of nuclear calcium-CREB-ATF3 activated by synaptic NMDA receptors defines a gene repression module that protects against extrasynaptic NMDA receptor-induced neuronal cell death and ischemic brain damage. *J Neurosci*. 31(13):4978–4990.
- Zhang SJ, Steijaert MN, Lau D, Schütz G, Delucinge-Vivier C, Descombes P, Bading H. 2007. Decoding NMDA receptor signaling: identification of genomic programs specifying neuronal survival and death. *Neuron*. 53:549–562.
- Zhang SJ, Zou M, Lu L, Lau D, Ditzel DA, Delucinge-Vivier C, Aso Y, Descombes P, Bading H. 2009. Nuclear calcium signaling controls expression of a large gene pool: identification of a gene program for acquired neuroprotection induced by synaptic activity. *PLoS Genet*. 5(8):e1000604.